Chapter 3

One-Dimensional Systems

In this chapter we describe geometrical methods of analysis of one-dimensional dynamical systems, i.e., systems having only one variable. An example of such a system is the space-clamped membrane having Ohmic leak current I_L

$$C\dot{V} = -g_L(V - E_L) \,. \tag{3.1}$$

Here the membrane voltage V is a time-dependent variable, and the capacitance C, leak conductance g_L and leak reverse potential E_L are constant parameters described in the previous chapter. We use this and other one-dimensional neural models to introduce and illustrate the most important concepts of dynamical system theory: equilibrium, stability, attractor, phase portrait, and bifurcation.

3.1 Electrophysiological Examples

The Hodgkin-Huxley description of dynamics of membrane potential and voltage-gated conductances can be reduced to a one-dimensional system when all transmembrane conductances have fast kinetics. For the sake of illustration, let us consider a space-clamped membrane having leak current and a fast voltage-gated current I_{fast} having only one gating variable p,

$$
\begin{aligned}
C\dot{V} &= -\overbrace{g_L(V - E_L)}^{\text{Leak } I_L} - \overbrace{g\,p\,(V - E)}^{I_{fast}} & (3.2) \\
\dot{p} &= (p_\infty(V) - p)/\tau(V) & (3.3)
\end{aligned}
$$

with dimensionless parameters $C = 1$, $g_L = 1$, and $g = 1$. Suppose that the gating kinetic (3.3) is much faster than the voltage kinetic (3.2), which means that the voltage-sensitive time constant $\tau(V)$ is very small, i.e. $\tau(V) \ll 1$, in the entire biophysical voltage range. Then, the gating process may be treated as being instantaneous, and the asymptotic value $p = p_\infty(V)$ may be used in the voltage equation (3.2) to reduce
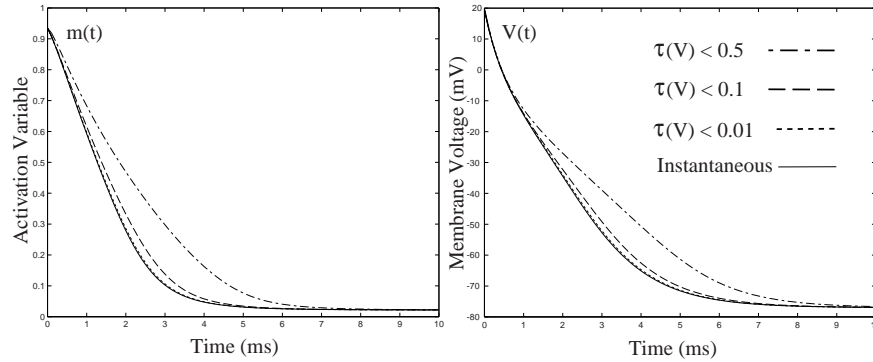
Figure 3.1: Solution of the full system (3.2, 3.3) converges to that of the reduced one-dimensional system (3.4) as $\tau(V) \to 0$

the two-dimensional system (3.2, 3.3) to a one-dimensional equation

$$C\,\dot{V} = -g_{\mathrm{L}}(V - E_{\mathrm{L}}) - \overbrace{g\,p_\infty(V)\,(V - E)}^{\text{instantaneous } I_{\text{fast}}}\ . \tag{3.4}$$

This reduction introduces a small error of the order $\tau(V) \ll 1$, as one can see in Fig. 3.1.

Since the hypothetical current I_{fast} can be either inward ($E > E_{\mathrm{L}}$) or outward ($E < E_{\mathrm{L}}$), and the gating process can be either activation (p is m, as in Hodgkin-Huxley model) or inactivation (p is h), there are four fundamentally different choices for $I_{\text{fast}}(V)$, which we summarize in Fig. 3.2 and elaborate below.

Figure 3.2: Four fundamental examples of voltage-gated currents having one gating variable. In this book we treat "hyperpolarization-activated" currents I_{h} and I_{Kir} as being inactivating currents, which are turned off (inactivated via h) by depolarization and turned on (deinactivated) by hyperpolarization; see discussion in Sect. 2.2.4.

3.1.1   I-V relations and dynamics

The four choices in Fig. 3.2 result in four simple one-dimensional models of the form (3.4)

$$I_{\mathrm{Na,p}}\text{-}model\,, \qquad I_{\mathrm{K}}\text{-}model\,, \qquad I_{\mathrm{h}}\text{-}model\,, \quad \text{and} \quad I_{\text{Kir}}\text{-}model\,.$$

These models might seem to be too simple for biologists, who can easily understand their behavior just by looking at the I-V relations of the currents depicted in Fig. 3.3
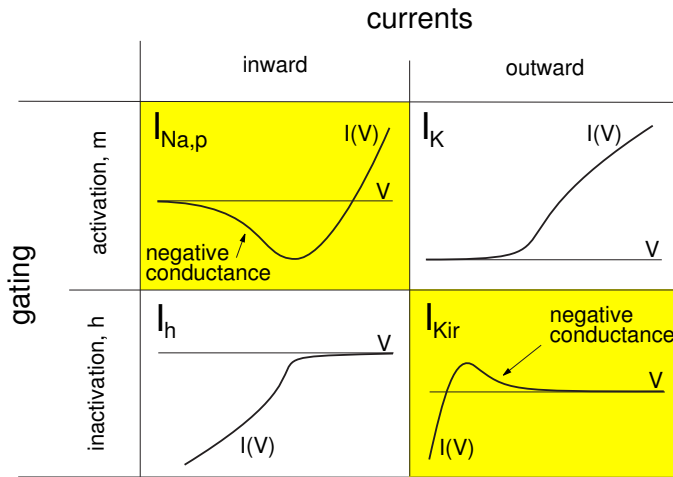
Figure 3.3: Typical current-voltage (I-V) relations of the four currents considered in this chapter. Shaded boxes correspond to non-monotonic I-V relations having a region of negative conductance ($I'(V) < 0$) in the biophysically relevant voltage range.

without using any dynamical systems theory. The models might also appear too simple for mathematicians, who can easily understand their dynamics just by looking at the graphs of the right-hand side of (3.4) without using any electrophysiological intuition. In fact, the models provide an invaluable learning tool, since they establish a bridge between electrophysiology and dynamical systems.

In Fig. 3.3 we plot typical steady-state current-voltage (I-V) relations of the four currents considered above. Notice that the I-V curve is non-monotonic for $I_{\mathrm{Na,p}}$ and I_{Kir} but monotonic for I_{K} and I_{h}, at least in the biophysically relevant voltage range. This subtle difference is an indication of the fundamentally different roles these currents play in neuron dynamics: The I-V relation in the first group has a region of "negative conductance", i.e., $I'(V) < 0$, which creates positive feedback between the voltage and the gating variable (Fig. 3.4), and it plays an amplifying role in neuron dynamics. We refer to such currents as being *amplifying currents*. In contrast, the currents in the second group have negative feedback between voltage and gating variable, and they often result in damped oscillation of the membrane potential, as we show in the next chapter. We refer to such currents as being *resonant currents*. Most neural models involve a combination of at least one amplifying and one resonant current, as we discuss in Chap. 5. The way these currents are combined determines whether the neuron is an *integrator* or a *resonator*.

3.1.2 Leak + instantaneous $I_{\mathrm{Na,p}}$

To ease our introduction into dynamical systems, we will use the $I_{\mathrm{Na,p}}$-model

$$C\dot{V} = I - g_{\mathrm{L}}(V - E_{\mathrm{L}}) - \overbrace{g_{\mathrm{Na}}\, m_{\infty}(V)\, (V - E_{\mathrm{Na}})}^{\text{instantaneous } I_{\mathrm{Na,p}}} \tag{3.5}$$

with

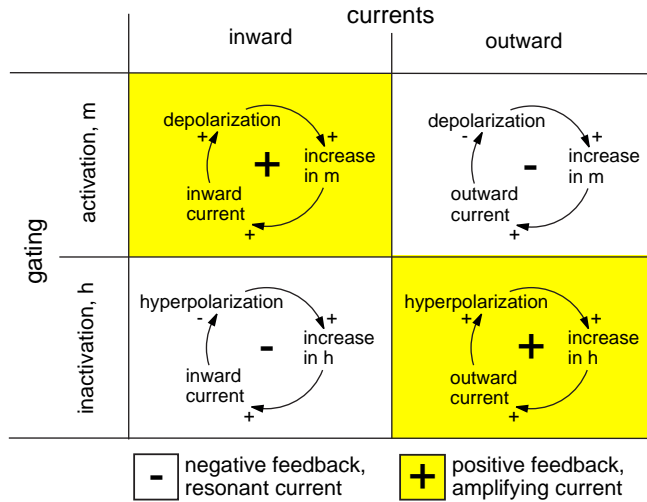$$m_{\infty}(V) = 1/(1 + \exp\{(V_{1/2} - V)/k\})$$

Figure 3.4: Feedback loops between voltage and gating variables in the four models presented above.

throughout the rest of this chapter. (Some biologists refer to transient Na$^+$ currents with very slow inactivation as being persistent, since the current does not change much on the time scale of 1 sec.) We measure the parameters

$$
\begin{array}{llll}
C = 10 \ \mu\text{F} & I = 0 \ \text{pA} & g_\text{L} = 19 \ \text{mS} & E_\text{L} = -67 \ \text{mV} \\
g_\text{Na} = 74 \ \text{mS} & V_{1/2} = 1.5 \ \text{mV} & k = 16 \ \text{mV} & E_\text{Na} = 60 \ \text{mV}
\end{array}
$$

using whole-cell patch clamp recordings of a layer 5 pyramidal neuron in visual cortex of a rat at room temperature. We prove in Ex. 3.3.8 and illustrate in Fig. 3.15 that the model approximates action potential upstroke dynamics of this neuron.

The model's I-V relation, $I(V)$, is depicted in Fig. 3.5a. Due to the negative conductance region in the I-V curve, this one-dimensional model can exhibit a number of interesting non-linear phenomena, such as bistability, i.e. co-existence of the resting and excited states. From mathematical point of view, bistability occurs because the right-hand side function of the differential equation (3.5), depicted in Fig. 3.5b, is not monotonic. In Fig. 3.6 we depict typical voltage time courses of the model (3.5) with two values of injected dc-current I and 16 different initial conditions. The qualitative behavior in Fig. 3.6a is apparently bistable: depending on the initial condition, the trajectory of the membrane potential goes either up to the excited state or down to the resting state. In contrast, the behavior in Fig. 3.6b is monostable, since the resting state does not exist. The goal of the dynamical system theory reviewed in this chapter is to understand why and how the behavior depends on the initial conditions and the parameters of the system.

3.2   Dynamical Systems

In general, dynamical systems can be continuous or discrete, depending on whether they are described by differential or difference equations. Continuous one-dimensional
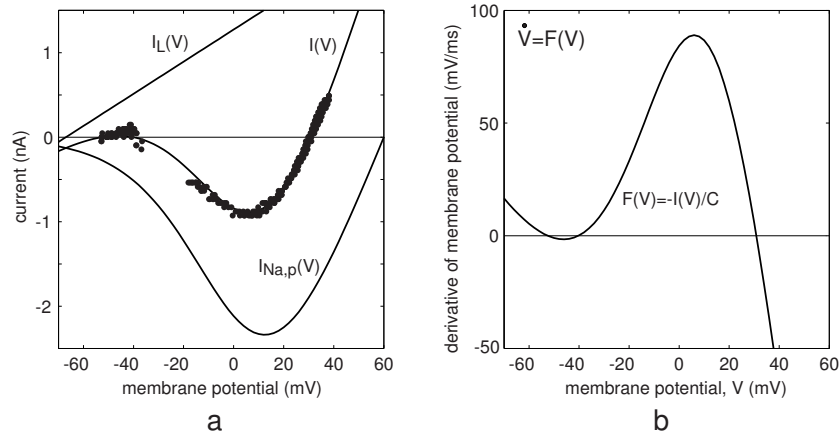
Figure 3.5: *a*. I-V relations of the leak current, I_L, fast Na$^+$ current, I_{Na}, and combined current $I(V) = I_L(V) + I_{Na}(V)$ in the $I_{Na,p}$-model (3.5). Dots denote $I_0(V)$ data from layer 5 pyramidal cell in rat visual cortex. *b*. The right-hand side of the $I_{Na,p}$-model (3.5).

dynamical systems are usually written in the form

$$\dot{V} = F(V) , \qquad V(0) = V_0 \in \mathbb{R} , \qquad (3.6)$$

for example,

$$\dot{V} = -80 - V , \qquad V(0) = -20 ,$$

where V is a scalar time-dependent variable denoting the current state of the system, $\dot{V} = V_t = dV/dt$ is its derivative with respect to time t, F is a scalar function (its output is one-dimensional) that determines the evolution of the system, e.g., the right-hand side of (3.5) divided by C; see Fig. 3.5b. $V_0 \in \mathbb{R}$ is an initial condition, and $\mathbb{R}$ is the real line, i.e., a line of real numbers ($\mathbb{R}^n$ would be the n-dimensional real space).

In the context of dynamical systems, the real line $\mathbb{R}$ is called *phase line* or *state line* (phase space or state space for $\mathbb{R}^n$) to stress the fact that each point in $\mathbb{R}$ corresponds to a certain perhaps inadmissible state of the system, and each state of the system corresponds to a certain point in $\mathbb{R}$. For example, the state of the Ohmic membrane (3.1) is just its membrane potential $V \in \mathbb{R}$. The state of the Hodgkin-Huxley model (see Sect. 2.3) is the four-dimensional vector $(V, m, n, h) \in \mathbb{R}^4$. The state of the $I_{Na,p}$-model (3.5) is again its membrane potential $V \in \mathbb{R}$, because the value $m = m_\infty(V)$ is unequivocally defined by V.

When all parameters are constant, then the dynamical system is called *autonomous*. When at least one of the parameters is time-dependent, the system is non-autonomous, denoted as $\dot{V} = F(V, t)$.

To solve (3.6) means to find a function $V(t)$ whose initial value is $V(0) = V_0$ and whose derivative is $F(V(t))$ at each moment $t \geq 0$. For example, the function $V(t) = V_0 + at$ is an explicit analytical solution to the dynamical system $\dot{V} = a$. The exponentially decaying function $V(t) = E_L + (V_0 - E_L)e^{-g_L t/C}$ depicted in Fig. 3.7,
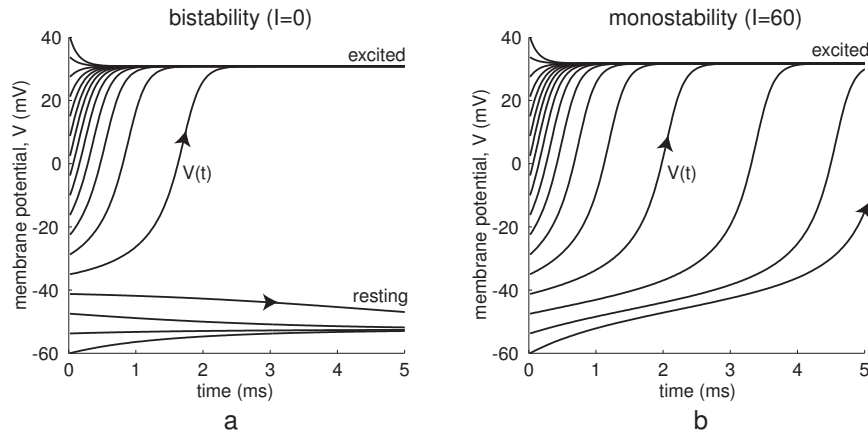
Figure 3.6: Typical voltage trajectories of the $I_{\text{Na,p}}$-model (3.5) having different values of I.
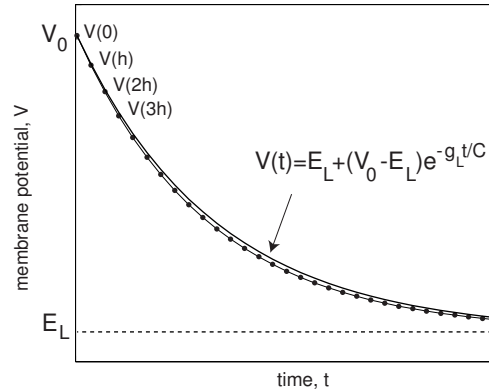

Figure 3.7: Explicit analytical solution $(V(t) = E_{\text{L}} + (V_0 - E_{\text{L}})e^{-g_{\text{L}}t/C})$ of linear equation (3.1) and corresponding numerical approximation (dots) using Euler method (3.7).

solid curve, is an explicit analytical solution to the linear equation (3.1) (check by differentiating).

Finding explicit solutions is often impossible even for such simple systems as (3.5), so most quantitative analysis is carried out via numerical simulations. The simplest procedure to solve (3.6) numerically, known as first-order *Euler method*, substitutes (3.6) by the discretized system

$$(V(t + h) - V(t))/h = F(V(t))$$

where $t = 0, h, 2h, 3h, \ldots$, is the discrete time and h is a small time step. Knowing the current state $V(t)$, we can find the next state point via

$$V(t + h) = V(t) + hF(V(t)) \ . \tag{3.7}$$

Iterating this *difference* equation starting with $V(0) = V_0$, we can approximate the analytical solution of (3.6), see dots in Fig. 3.7. The approximation has a noticeable error
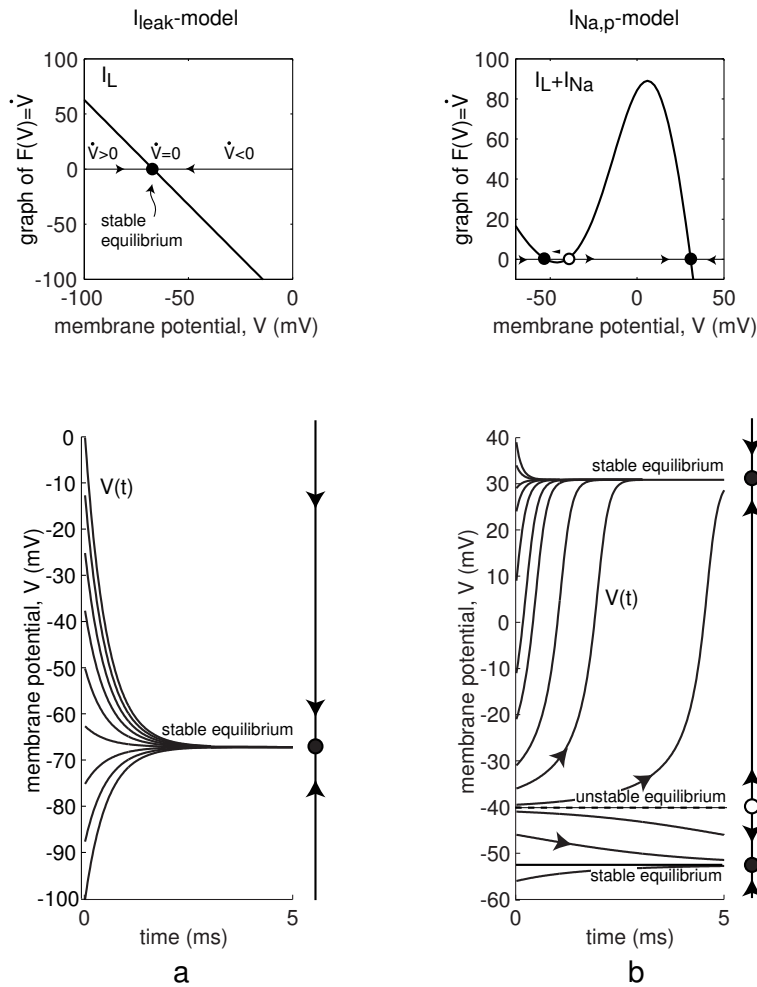
Figure 3.8: Graphs of the right-hand side functions of equations (3.1) and (3.5) and corresponding numerical solutions starting from various initial conditions.

of order h, so scientific software packages, such as MATLAB, use more sophisticated high-precision numerical methods.

In many cases, however, we do not need exact solutions, but rather qualitative understanding of the behavior of (3.6) and how it depends on parameters and the initial state V_0. For example, we might be interested in the number of equilibrium (rest) points the system could have, whether the equilibria are stable, their attraction domains, etc.

3.2.1 Geometrical analysis

The first step in qualitative geometrical analysis of any one-dimensional dynamical system is to plot the graph of the function F, as we do in Fig. 3.8,top. Since $F(V) = \dot{V}$, at every point V where $F(V)$ is negative, the derivative $\dot{V}$ is negative, and hence the

state variable V decreases. In contrast, at every point where $F(V)$ is positive, $\dot{V}$ is positive, and the state variable V increases; the greater the value of $F(V)$, the faster V increases. Thus, the direction of movement of the state variable V, and hence the evolution of the dynamical system, is determined by the sign of the function $F(V)$.

The right-hand side of the I_{leak}-model (3.1) or the $I_{\text{Na,p}}$-model (3.5) in Fig. 3.8 is the steady-state current-voltage (I-V) relation, $I_{\text{L}}(V)$ or $I_{\text{L}}(V)+I_{\text{Na,p}}(V)$ respectively, taken with the minus sign, see Fig. 3.5. Positive values of the right-hand side $F(V)$ mean negative I-V corresponding to the net inward current that depolarizes the membrane. Conversely, negative values mean positive I-V corresponding to the net outward current that hyperpolarizes the membrane.

3.2.2   Equilibria

The next step in qualitative analysis of any dynamical system is to find its *equilibria* or *rest points*, i.e., the values of the state variable where

$$F(V) = 0 \qquad (V \text{ is an equilibrium}).$$

At each such point $\dot{V} = 0$, the state variable V does not change. In the context of membrane potential dynamics, equilibria correspond to the points where the steady-state I-V curve passes zero. At each such point there is a balance of the inward and outward currents so that the net transmembrane current is zero, and the membrane voltage does not change. (Incidentally, the part $l\bar{i}bra$ in the Latin word $aequil\bar{i}brium$ means balance).

The I_{K}- and I_{h}-models mentioned in Sect. 3.1 can have only one equilibrium because their I-V relations $I(V)$ are monotonic increasing functions. The corresponding functions $F(V)$ are monotonic decreasing and can have only one zero.

In contrast, the $I_{\text{Na,p}}$- and I_{Kir}-models can have many equilibria because their I-V curves are not monotonic, and hence there is a possibility for multiple intersections with the V-axis. For example, there are three equilibria in Fig. 3.8b corresponding to the rest state (around -53 mV), threshold state (around -40 mV) and the excited state (around 30 mV). Each equilibrium corresponds to the balance of the outward leak current and partially (rest), moderately (threshold) or fully (excited) activated persistent Na$^+$ inward current. Throughout this book we denote equilibria as small open or filled circles depending on their stability, as in Fig. 3.8.

3.2.3   Stability

If the initial value of the state variable is exactly at equilibrium, then $\dot{V} = 0$ and the variable will stay there forever. If the initial value is near the equilibrium, the state variable may approach the equilibrium or diverge from it. Both cases are depicted in Fig. 3.8. We say that an equilibrium is *asymptotically stable* if all solutions starting sufficiently near the equilibrium will approach it as $t \to \infty$.
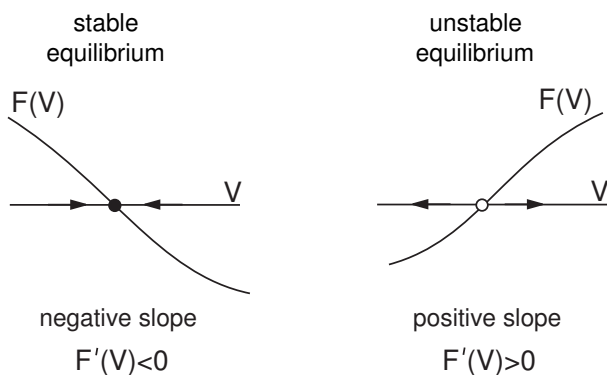
Figure 3.9: The sign of the slope, $\lambda = F'(V)$, determines the stability of the equilibrium.

Stability of an equilibrium is determined by the signs of the function F around it. The equilibrium is stable when $F(V)$ changes the sign from "+" to "−" as V increases, as in Fig. 3.8a. Obviously, all solutions starting near such an equilibrium converge to it. Such an equilibrium "attracts" all nearby solutions, and it is called an *attractor*. A stable equilibrium point is the only type of attractor that can exist in one-dimensional continuous dynamical systems defined on a state line $\mathbb{R}$. Multidimensional systems can have other attractors, e.g., limit cycles.

The differences between stable, asymptotically stable, and exponentially stable equilibria are discussed in Ex. 19 in the end of the chapter. The reader is also encouraged to solve Ex. 4 (piece-wise continuous $F(V)$).

3.2.4 Eigenvalues

A sufficient condition for an equilibrium to be stable is that the derivative of the function F with respect to V at the equilibrium is negative, provided that the function is differentiable. We denote such a derivative here by the Greek letter

$$\lambda = F'(V) , \qquad (V \text{ is an equilibrium; that is, } F(V) = 0)$$

and note that it is just the slope of graph of F at the point V; see Fig. 3.9. Obviously, when the slope, λ, is negative, the function changes the sign from "+" to "−", and the equilibrium is stable. Positive slope λ implies instability. The parameter λ defined above is the simplest example of an *eigenvalue* of an equilibrium. We introduce eigenvalues formally in the next chapter and show that eigenvalues play an important role in defining the types of equilibria of multi-dimensional systems.

3.2.5 Unstable equilibria

If a one-dimensional system has two stable equilibrium points, then they must be separated by at least one unstable equilibrium point, as we illustrate in Fig. 3.10. (This may not be true in multidimensional systems.) Indeed, a continuous function F has to change the sign from "−" to "+" somewhere in between those equilibria; that is, it has to cross the V axis in some point, as in Fig. 3.8b. This point would be
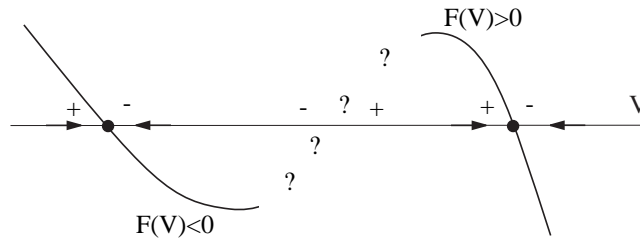
Figure 3.10: Two stable equilibrium points must be separated by at least one unstable equilibrium point because $F(V)$ has to change the sign from "$-$" to "$+$".

an unstable equilibrium, since all nearby solutions diverge from it. In the context of neuronal models, unstable equilibria correspond to the region of the steady-state I-V curve with negative conductance. (Please, check that this is in accordance with the fact that $F(V) = -I(V)/C$; see Fig. 3.5.) An unstable equilibrium is sometimes called a *repeller*. Attractors and repellers have a simple mechanistic interpretation depicted in Fig. 3.11.

If the initial condition V_0 is set to an unstable equilibrium point, then the solution will stay at this unstable equilibrium; i.e., $V(t) = V_0$ for all t, at least in theory. In practice, the location of an equilibrium point is known only approximately. In addition, small noisy perturbations that are always present in biological systems can make $V(t)$ deviate slightly from the equilibrium point. Because of instability, such deviations will grow, and the state variable $V(t)$ will eventually diverge form the repelling equilibrium the same way as the ball set at the top of the hill in Fig. 3.11 will eventually roll downhill. If the level of noise is low, it could take a long time to diverge from the repeller.

3.2.6   Attraction domain

Even though unstable equilibria are hard to see experimentally, they still play an important role in dynamics, since they separate attraction domains. Indeed, the ball in Fig. 3.11 could go left or right depending on what side of the hilltop it is on initially. Similarly, the state variable of a one-dimensional system decreases or increases depending on what side of the unstable equilibrium the initial condition is, as one can clearly see in Fig. 3.8b.

In general, a *basin of attraction* or *attraction domain* of an attractor is the set of all initial conditions that lead to the attractor. For example, the attraction domain of the equilibrium in Fig. 3.8a is the entire voltage range. Such an attractor is called *global*. In Fig. 3.12 we plot attraction domains of two stable equilibria. The middle unstable equilibrium is always the boundary of the attraction domains.
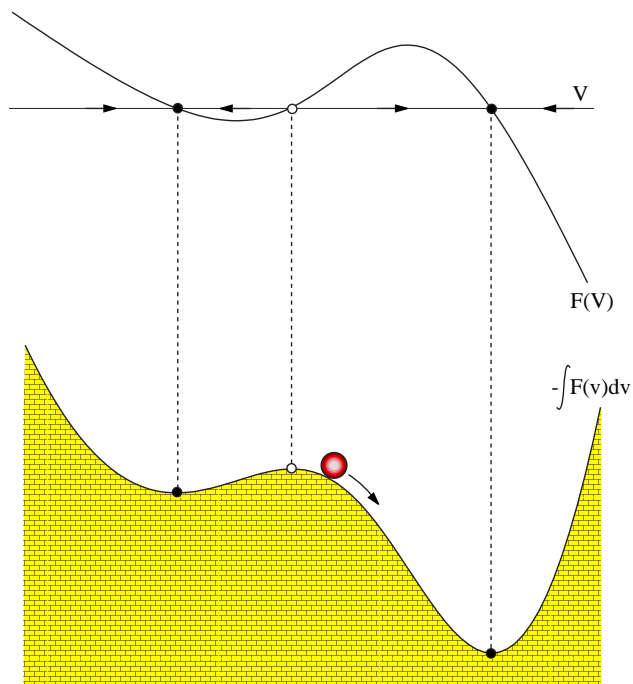
Figure 3.11: Mechanistic interpretation of stable and unstable equilibria. A massless (inertia free) ball moves toward energy minima with the speed proportional to the slope. A one-dimensional system $\dot{V} = F(V)$ has the energy landscape $E(V) = -\int_{-\infty}^{V} F(v)\, dv$; see Ex. 18. Zeros of $F(V)$ with negative (positive) slope correspond to minima (maxima) of $E(V)$.

3.2.7 Threshold and action potential

Unstable equilibria play the role of thresholds in one-dimensional bistable systems, i.e., in systems having two attractors. We illustrate this in Fig. 3.13, which is believed to describe the essence of the mechanism of bistability in many neurons. Suppose the state variable is initially at the stable equilibrium point marked as "state A" in the figure, and suppose that perturbations can kick it around the equilibrium. Small perturbations may not kick it over the unstable equilibrium so that the state variable continues to be in the attraction domain of the "state A". We refer to such perturbations as being *subthreshold*. In contrast, we refer to perturbations as being *superthreshold* (also known as *suprathreshold*) if they are large enough to push the state variable over the unstable equilibrium so that it becomes attracted to the "state B". We see that the unstable equilibrium acts as a threshold that separates two states.

The transition between two stable states separated by a threshold is relevant to the mechanism of excitability and generation of action potentials by many neurons, which we illustrate in Fig. 3.14. In the $I_{\text{Na,p}}$-model (3.5) with the I-V relation in Fig. 3.5 the existence of the rest state is largely due to the leak current I_{L}, while the existence of the excited state is largely due to the persistent inward Na^{+} current $I_{\text{Na,p}}$. Small
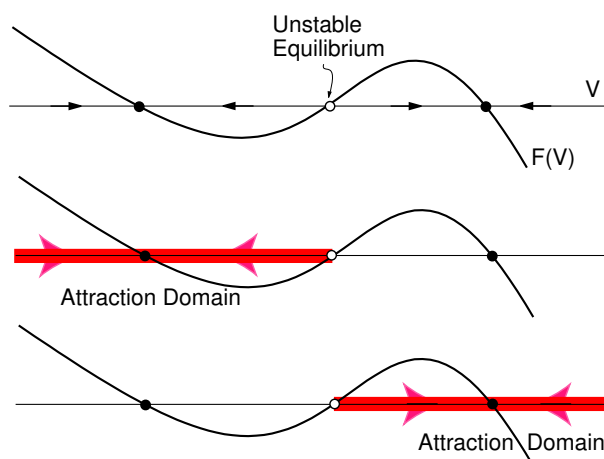
Figure 3.12: Two attraction domains in a one-dimensional system are separated by the unstable equilibrium.

(subthreshold) perturbations leave the state variable in the attraction domain of the rest state, while large (superthreshold) perturbations initiate the regenerative process — the upstroke of an action potential, and the voltage variable becomes attracted to the excited state. Generation of the action potential must be completed via repolarization that moves V back to the rest state. Typically, repolarization occurs because of a relatively slow inactivation of Na^+ current and/or slow activation of an outward K^+ current, which are not taken into account in the one-dimensional system (3.5). To account for such processes, we consider two-dimensional systems in the next chapter.

   Recall that the parameters of the $I_{Na,p}$-model (3.5) were obtained from a cortical pyramidal neuron. In Fig. 3.15, left, we stimulate (*in vitro*) the cortical neuron by short (0.1 ms) strong pulses of current to reset its membrane potential to various initial values and interpret the results using the $I_{Na,p}$-model. Since activation of Na^+ current is not instantaneous in real neurons, we allow variable m to converge to $m_\infty(V)$, and ignore the 0.3-ms transient activity that follows each pulse. We also ignore the initial segment of the downstroke of the action potential, and plot the magnification of the voltage traces in Fig. 3.15, right. Comparing this figure with Fig. 3.8b, we see that the $I_{Na,p}$-model is a reasonable one-dimensional approximation of the action potential upstroke dynamics; It predicts the value of the resting (-53 mV), instantaneous threshold (-40 mV), and the excited (+30 mV) states of the cortical neuron.

3.2.8   Bistability and hysteresis

Systems having two (many) co-existing attractors are called *bistable* (*multi-stable*). Many neurons and neuronal models, such as the Hodgkin-Huxley model, exhibit bistability between resting (equilibrium) and spiking (limit cycle) attractors. Some neurons can exhibit bistability of two stable resting states in the subthreshold voltage range, e.g., -59 mV and -75 mV in the thalamocortical neurons (Hughes et al. 1999) depicted
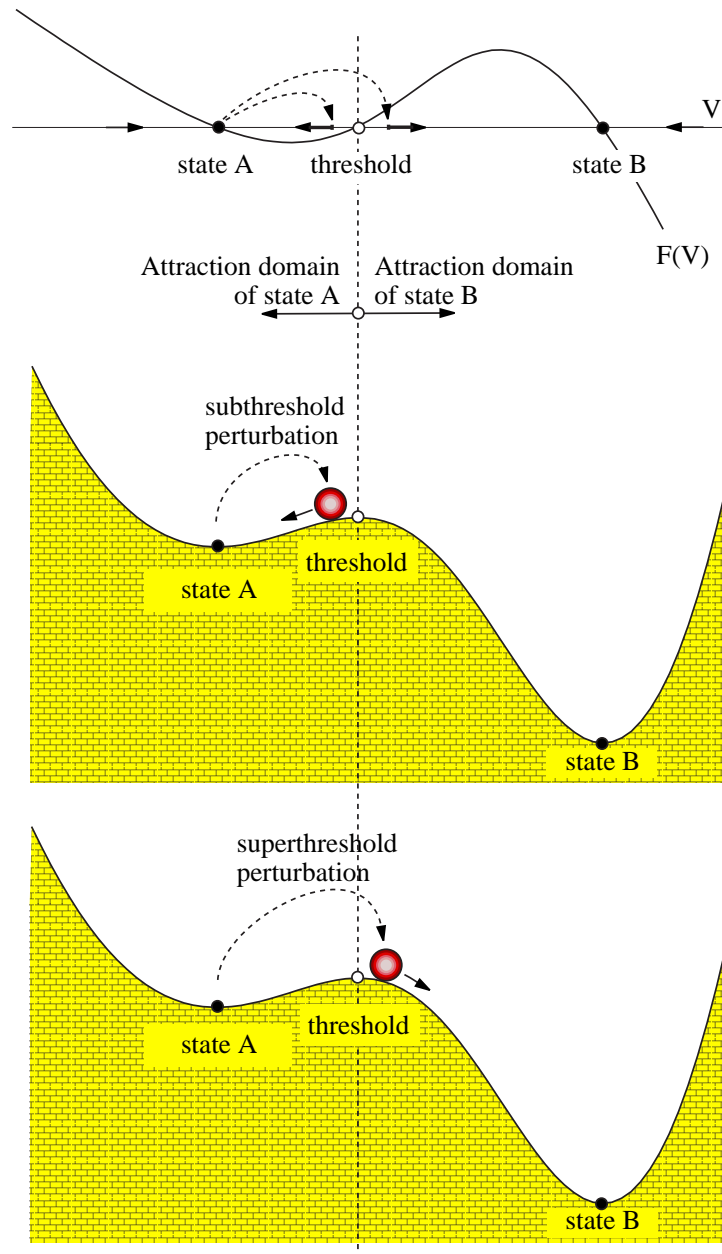
Figure 3.13: Unstable equilibrium plays the role of a threshold that separates two attraction domains.
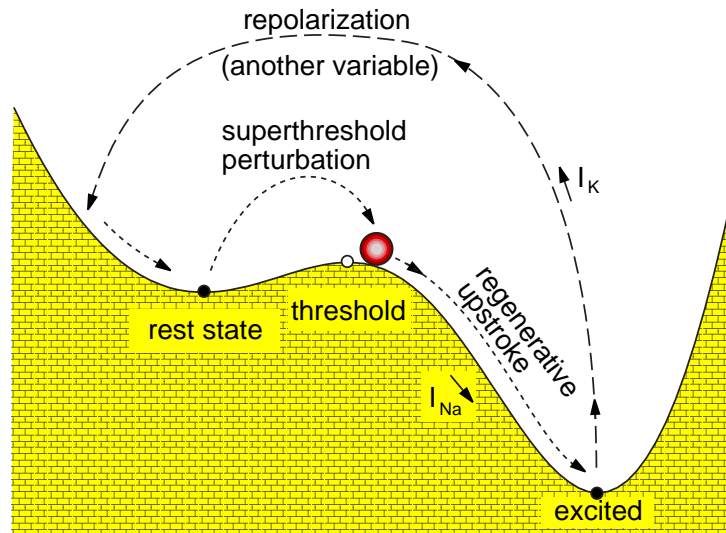
Figure 3.14: Mechanistic illustration of the mechanism of generation of an action potential.
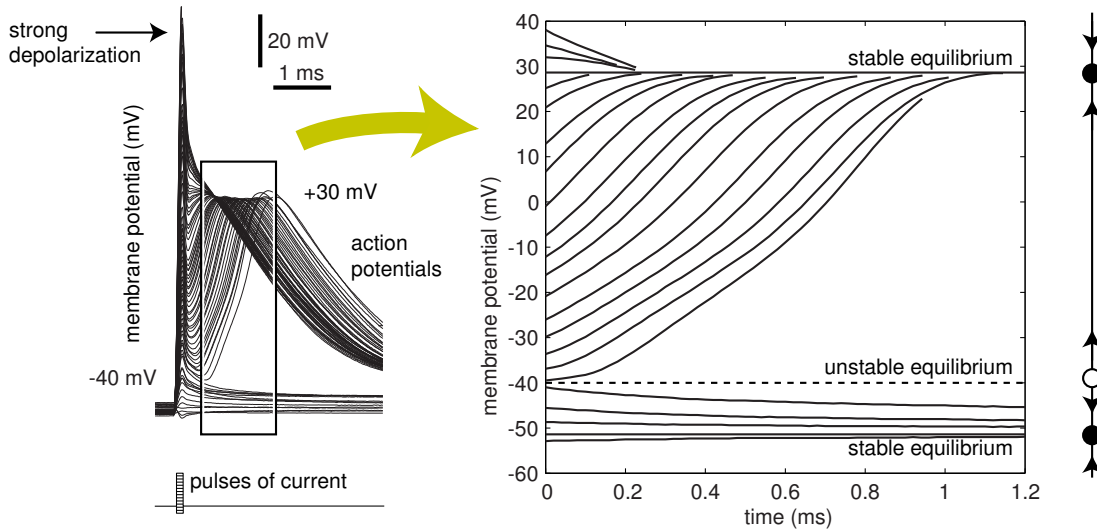

Figure 3.15: Upstroke dynamics of layer 5 pyramidal neuron *in vitro* (compare with the $I_{\mathrm{Na,p}}$-model (3.5) in Fig. 3.8b).
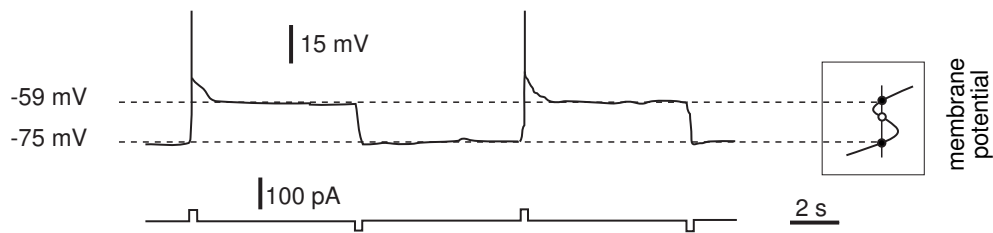
Figure 3.16: Membrane potential bistability in a cat TC neuron in the presence of ZD7288 (pharmacological blocker of I_h; modified from Fig. 6B of Hughes et al. 1999).
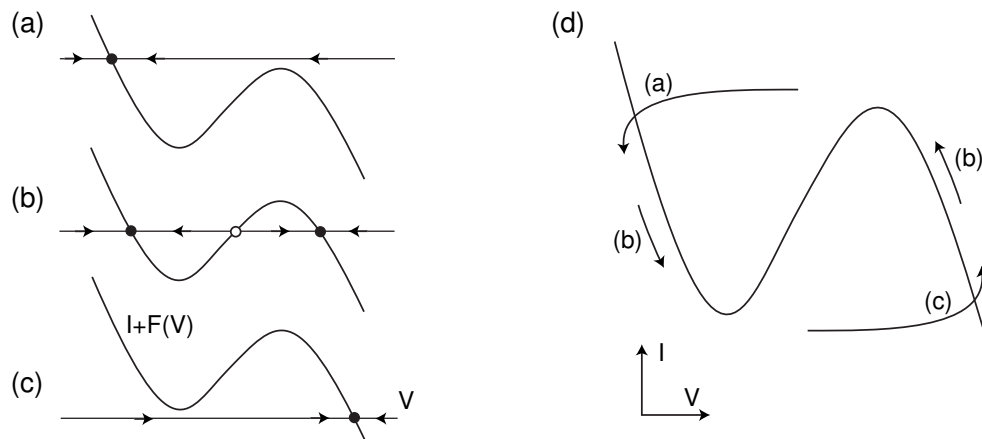

Figure 3.17: Bistability and hysteresis loop as I changes.

in Fig. 3.16, or -50 mV and -60 mV in mitral cells of olfactory bulb (Heyward et al. 2001), or -45 mV and -60 mV in Purkinje neurons. Brief inputs can switch such neurons from one state to the other, as in Fig. 3.16. Though the ionic mechanisms of bistability are different in the three neurons, the mathematical mechanism is the same.

Consider a one-dimensional system $\dot{V} = I + F(V)$ with function $F(V)$ having a cubic N-shape. Injection of a dc-current I shifts the function $I + F(V)$ up or down. When I is negative, the system has only one equilibrium depicted in Fig. 3.17a. As we remove the injected current I, the system is bistable as in Fig. 3.17b, but its state is still at the left equilibrium. As we inject positive current, the left stable equilibrium disappears via another saddle-node bifurcation, and the state of the system jumps to the right equilibrium, as in Fig. 3.17c. But as we slowly remove the injected current that caused the jump and go back to Fig. 3.17b, the jump to the left equilibrium does not occur until a much lower value corresponding to Fig. 3.17a. The failure of the system to return to the original value when the injected current is removed is called *hysteresis*. If I were a slow V-depended variable, then the system could exhibit relaxation oscillations depicted in Fig. 3.17d and described in the next chapter.
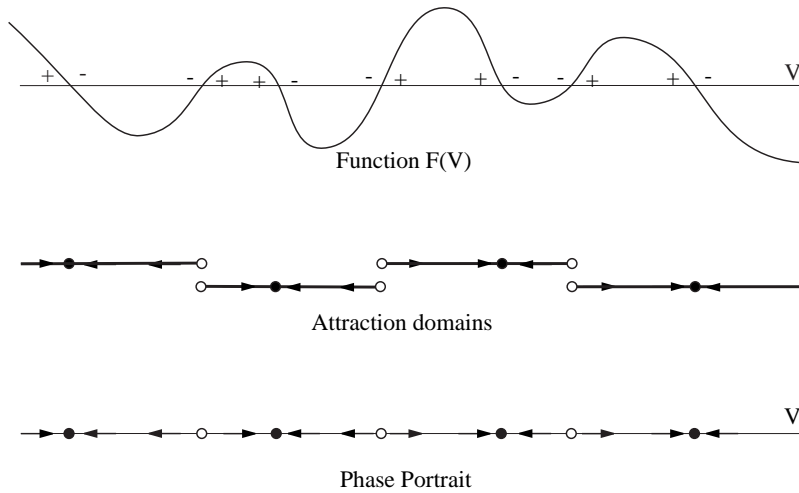
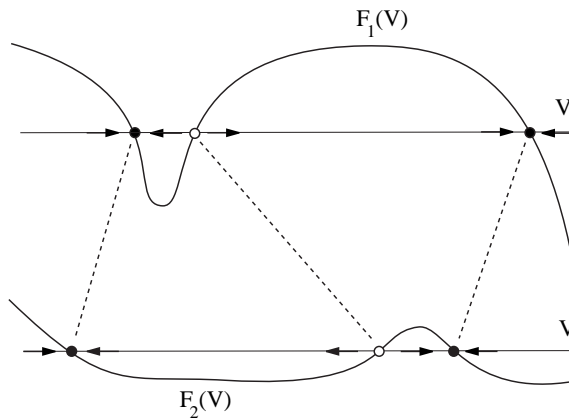Figure 3.18: Phase portrait of a one-dimensional system $\dot{V} = F(V)$.

Figure 3.19: Two "seemingly different" dynamical systems $\dot{V} = F_1(V)$ and $\dot{V} = F_2(V)$ are topologically equivalent, hence they have qualitatively similar dynamics.

3.3   Phase Portraits

An important component in qualitative analysis of any dynamical system is reconstruction of its *phase portrait*. For this one depicts all stable and unstable equilibria (as black and white circles respectively), representative trajectories, and corresponding attraction domains in the systems state/phase space, as we illustrate in Fig. 3.18. Phase portrait is a geometrical representation of system dynamics. It depicts all possible evolutions of the state variable and how they depend on the initial state. Looking at the phase portrait, one immediately gets all important information about the system qualitative behavior without even knowing the equation for F.
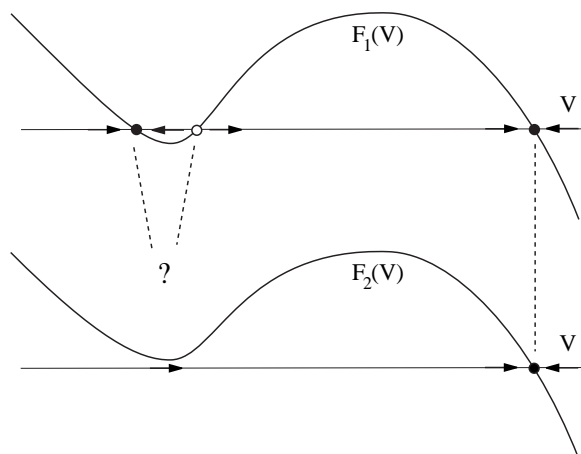
Figure 3.20: Two "seemingly alike" dynamical systems $\dot{V} = F_1(V)$ and $\dot{V} = F_2(V)$ are not topologically equivalent, hence they do not have qualitatively similar dynamics. (The first system has three equilibria, and the second system has only one.)

3.3.1 Topological equivalence

Phase portraits can be used to determine qualitative similarity of dynamical systems. In particular, two one-dimensional systems are said to be *topologically equivalent* when phase portrait of one of them treated as a piece of rubber can be stretched or shrunk to fit the other one, as in Fig. 3.19. Topological equivalence is a mathematical concept that clarifies the imprecise notion of "qualitative similarity", and its rigorous definition is provided, e.g., by Guckenheimer and Holmes (1983).

The stretching and shrinking of the "rubber" phase space are topological transformations that do not change the number of equilibria or their stability. Thus, two systems having different number of equilibria cannot be topologically equivalent, hence they have qualitatively different dynamics, as we illustrate in Fig. 3.20. Indeed, the top system is bistable because it has two stable equilibria separated by an unstable one. The evolution of the state variable depends on which attraction domain the initial condition is in initially. Such a system has "memory" of the initial condition. Moreover, sufficiently strong perturbations can switch it from one equilibrium state to another. In contrast, the bottom system in Fig. 3.20 has only one equilibrium, which is a global attractor, and the state variable converges to it regardless of the initial condition. Such a system has quite primitive dynamics, and it is topologically equivalent to the linear system (3.1).

3.3.2 Local equivalence and Hartman-Grobman theorem

In computational neuroscience, we usually face quite complicated systems describing neuronal dynamics. A useful strategy is to substitute such systems by simpler ones having topologically equivalent phase portraits. For example, both systems in Fig. 3.19 are topologically equivalent to $\dot{V} = V - V^3$ (please, check this), which is easier to deal with analytically.

Quite often we cannot find a simpler system that is topologically equivalent to our neuronal model on the entire state line $\mathbb{R}$. In this case, we make a sacrifice: we restrict
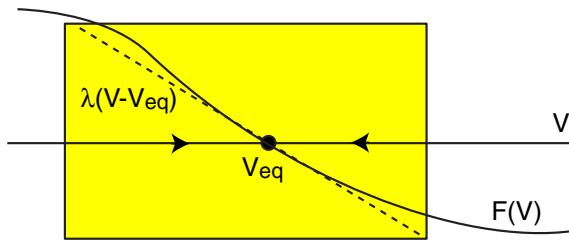
Figure 3.21: Hartman-Grobman theorem: Non-linear system $\dot{V} = F(V)$ is topologically equivalent to the linear one $\dot{V} = \lambda(V - V_{eq})$ in the local (shaded) neighborhood of the hyperbolic equilibrium V_{eq}.

our analysis to a small neighborhood of the line $\mathbb{R}$, e.g., the one containing the resting state or the threshold, and study behavior locally in this neighborhood.

An important tool in local analysis of dynamical systems is the Hartman-Grobman theorem, which says that a non-linear one-dimensional system

$$\dot{V} = F(V)$$

sufficiently near an equilibrium $V = V_{eq}$ is locally topologically equivalent to the linear one

$$\dot{V} = \lambda(V - V_{eq}) \tag{3.8}$$

provided that the eigenvalue

$$\lambda = F'(V_{eq})$$

at the equilibrium is non-zero, i.e., the slope of $F(V)$ is non-zero. Such an equilibrium is called *hyperbolic*. Thus, nonlinear systems near hyperbolic equilibria behave as if there were linear, as in Fig. 3.21.

It is easy to find the exact solution of the linearized system (3.8) with an initial condition $V(0) = V_0$. It is $V(t) = V_{eq} + e^{\lambda t}(V_0 - V_{eq})$ (check by differentiating). If the eigenvalue $\lambda < 0$, then $e^{\lambda t} \to 0$ and $V(t) \to V_{eq}$ as $t \to \infty$, so that the equilibrium is stable. Conversely, if $\lambda > 0$, then $e^{\lambda t} \to \infty$ meaning that the initial displacement, $V_0 - V_{eq}$, grows with the time, and the equilibrium is unstable. Thus, the linearization predicts qualitative dynamics at the equilibrium and quantitative rate of convergence/divergence to/from the equilibrium.

If the eigenvalue $\lambda = 0$, then the equilibrium is non-hyperbolic, and analysis of the linearized system $\dot{V} = 0$ cannot describe the behavior of the nonlinear system. Typically, non-hyperbolic equilibria arise when the system undergoes a bifurcation, i.e., a qualitative change of behavior, which we consider next. To study stability, we need to consider higher-order terms of the Taylor series of $F(V)$ at V_{eq}.

3.3.3 Bifurcations

The final and the most advanced step in qualitative analysis of any dynamical system is the bifurcation analysis. In general, a system is said to undergo a bifurcation when its phase portrait changes qualitatively. For example, the energy landscape in Fig. 3.22 changes so that the system is no longer bistable. Precise mathematical definition of a bifurcation will be given later.
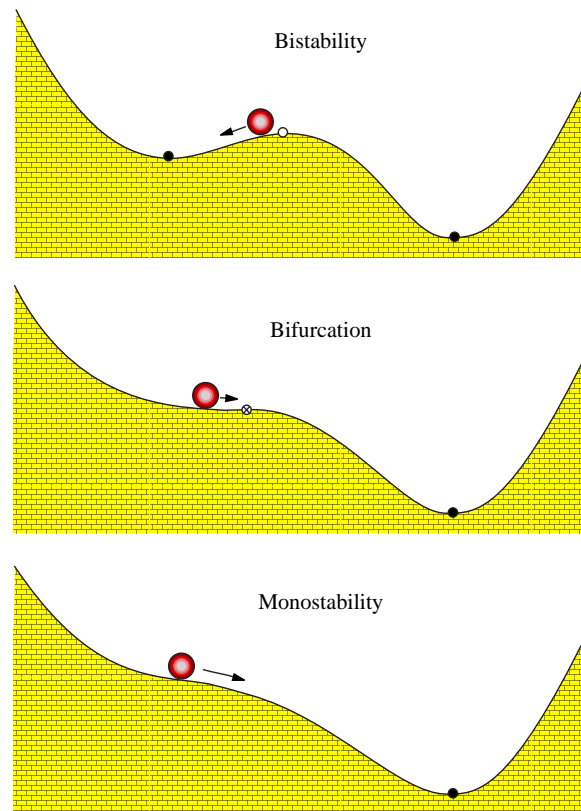
Figure 3.22: Mechanistic illustration of a bifurcation as a change of the landscape.

Qualitative change of the phase portrait may or may not necessarily reveal itself in a qualitative change of behavior, depending on the initial conditions. For example, there is a bifurcation in Fig. 3.23, left, but no change of behavior because the ball remains in the attraction domain of the right equilibrium. To see the change, we need to drop the ball at different initial conditions and observe the disappearance of the left equilibrium. In the same vain, there is no bifurcation Fig. 3.23, middle and right, (the phase portraits in each column are topologically equivalent) but the apparent change of behavior is caused by the expansion of the attraction domain of the left equilibrium or by the external input. Dropping the ball at different locations would result in the same qualitative picture – two stable equilibria whose attraction domains are separated by the unstable equilibrium. When mathematicians talk about bifurcations, they assume that all initial conditions could be sampled, in which case bifurcations do result in a qualitative change of behavior of the system as a whole.

To illustrate the importance of sampling all initial conditions, let us consider the *in vitro* recordings of a pyramidal neuron in Fig. 3.24. We inject 0.1-ms strong pulses of current of various amplitude to set the membrane potential to different initial values. Right after each pulse, we inject a 4 ms step of dc-current of amplitude $I = 0$, $I = 16$ or $I = 60$ pA. The case $I = 0$ pA is the same as in Fig. 3.15, so some initial conditions
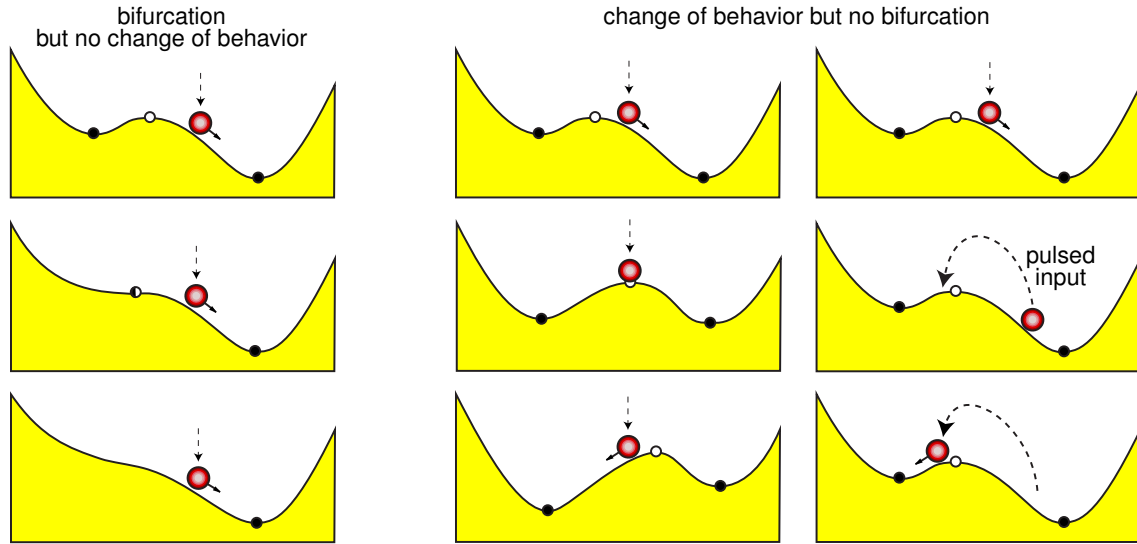
Figure 3.23: Bifurcations are not equivalent to qualitative change of behavior if the system is started with the same initial condition or subject to external input.
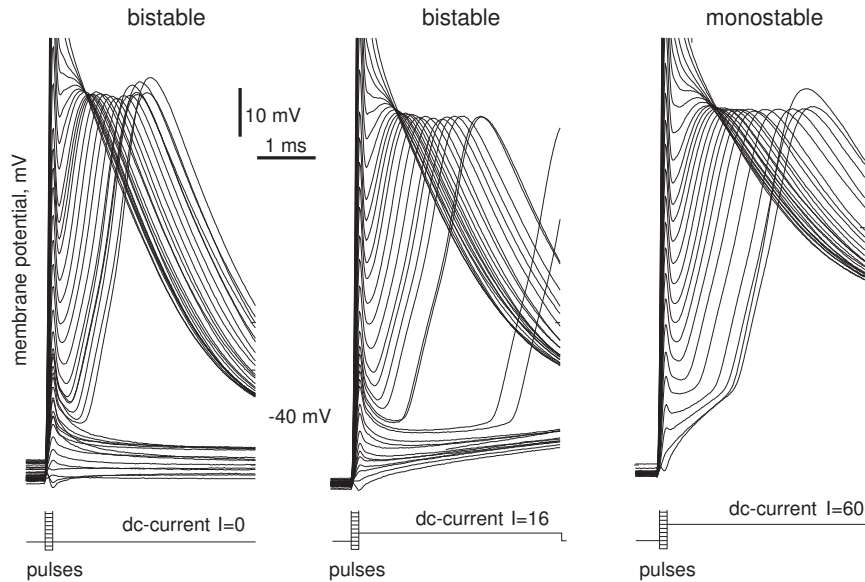

Figure 3.24: Qualitative change of the up-stroke dynamics of layer 5 pyramidal neuron from rat visual cortex (the same neuron as in Fig. 3.15).

result in upstroke of the action potential, while others do not. When $I = 60$ pA, all initial conditions result in the generation of an action potential. Apparently, a change of qualitative behavior occurs for some I between 0 and 60.

To understand the qualitative dynamics in Fig. 3.24, we consider the one-dimensional $I_{\mathrm{Na,p}}$-model (3.5) having different values of the parameter I and depict its trajectories in Fig. 3.25. One can clearly see that the qualitative behavior of the model depends on whether I is greater or less than 16. When $I = 0$ (top of Fig. 3.25), the system is bistable. The rest and the excited states coexist. When I is large (bottom of Fig. 3.25) the rest state no longer exists because leak outward current cannot cope with large injected dc-current I and the inward Na$^+$ current.

What happens when we change I past 16? The answer lies in the details of the geometry of the right-hand side function $F(V)$ of (3.5) and how it depends on the parameter I. Increasing I elevates the graph of $F(V)$. The higher the graph of $F(V)$ is, the closer its intersections with the V-axis are, as we illustrate in Fig. 3.26 depicting only the low-voltage range of the system. When I approaches 16, the distance between the stable and unstable equilibria vanishes; the equilibria coalesce and annihilate each other. The value $I = 16$ at which the equilibria coalesce is called the *bifurcation value*. This value separates two qualitatively different regimes: When I is near but less than 16, the system has three equilibria and bistable dynamics. The quantitative features, such as the exact locations of the equilibria depend on the particular values of I, but qualitative behavior remains unchanged no matter how close I to the bifurcation value is. In contrast, when I is near but greater than 16 the system has only one equilibrium and monostable dynamics.

In general, a dynamical system may depend on a vector of parameters, say p. A point in the parameter space, say $p = a$, is said to be a *regular* or non-bifurcation point, if the system's phase portrait at $p = a$ is topologically equivalent to the phase portrait at $p = c$ for any c sufficiently near a. For example, the value $I = 13$ in Fig. 3.26 is regular, since the system has topologically equivalent phase portraits for all I near 13. Similarly, the value $I = 18$ is also regular. Any point in the parameter space that is not regular is called a bifurcation point. Namely, a point $p = b$ is a bifurcation point, if the system's phase portrait at $p = b$ is not topologically equivalent to the phase portrait at some point $p = c$ no matter how close c to b is. The value $I = 16$ in Fig. 3.26 is a bifurcation point. It corresponds to the *saddle-node* (also known as *fold* or *tangent*) bifurcation for reasons described later. It is one of the simplest bifurcations considered in this book.

3.3.4   Saddle-node (fold) bifurcation

In general, a one-dimensional system

$$\dot{V} = F(V, I)$$

having an equilibrium point $V = V_{\mathrm{sn}}$ for some value of the parameter $I = I_{\mathrm{sn}}$ (i.e., $F(V_{\mathrm{sn}}, I_{\mathrm{sn}}) = 0$) is said to be at a *saddle-node* bifurcation (sometimes called a *fold*
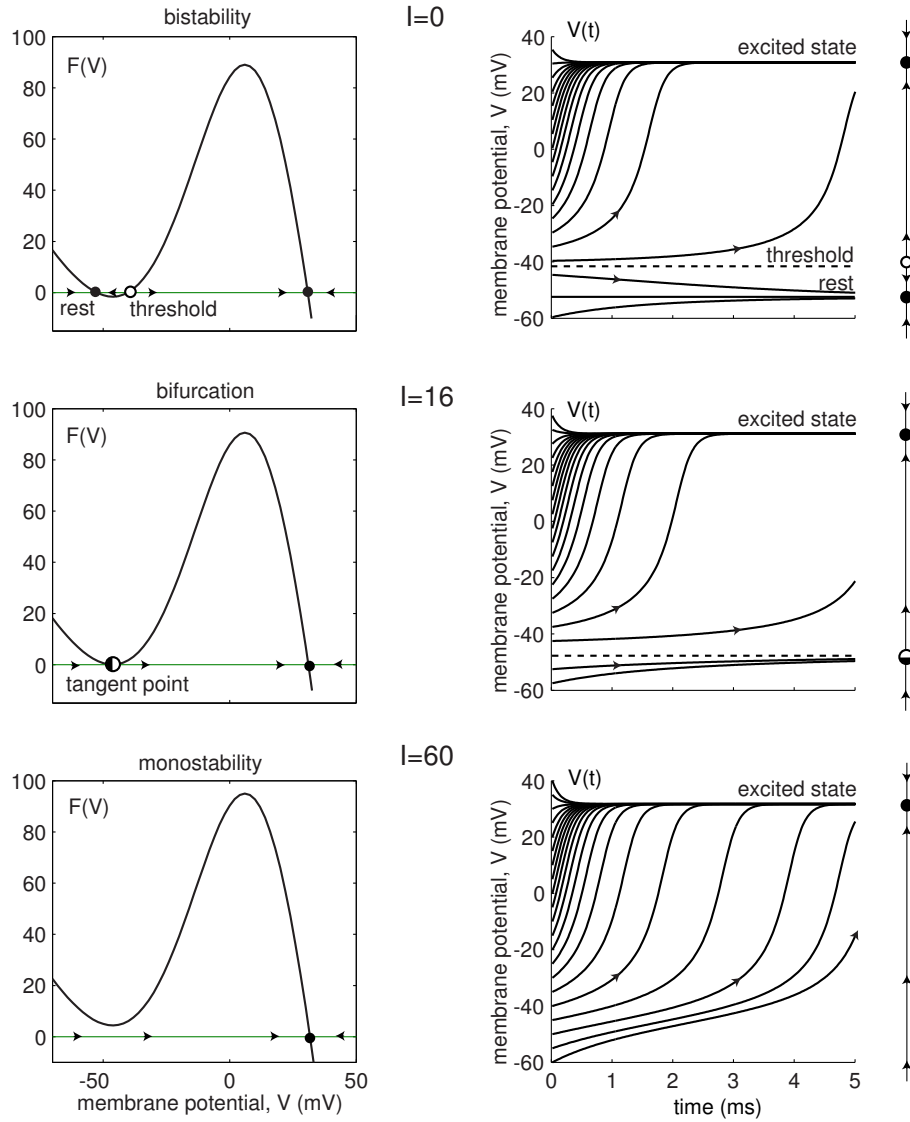
Figure 3.25: Bifurcation in the $I_{\mathrm{Na,p}}$-model (3.5): The rest state and the threshold state coalesce and disappear when the parameter I increases.
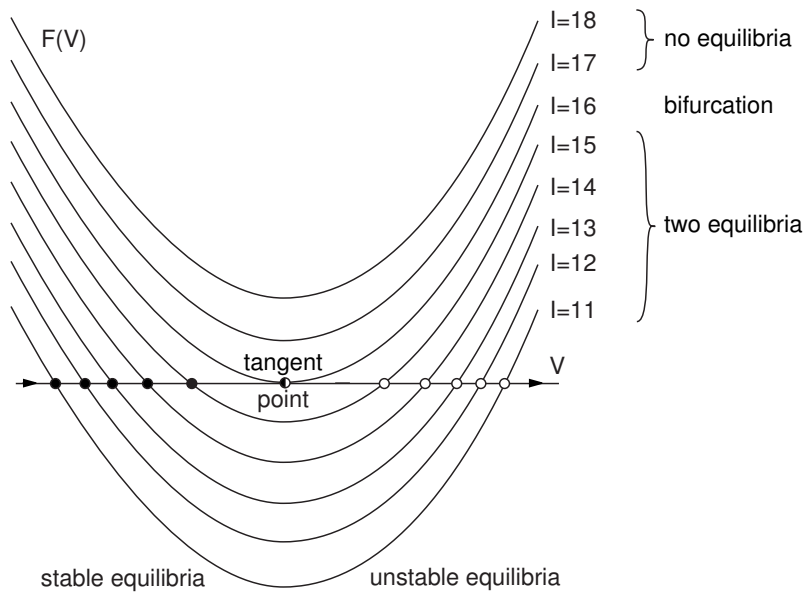
Figure 3.26: Saddle-node bifurcation: While the graph of the function $F(V)$ is lifted up, the stable and unstable equilibria approach each other, coalesce at the tangent point, and then disappear.
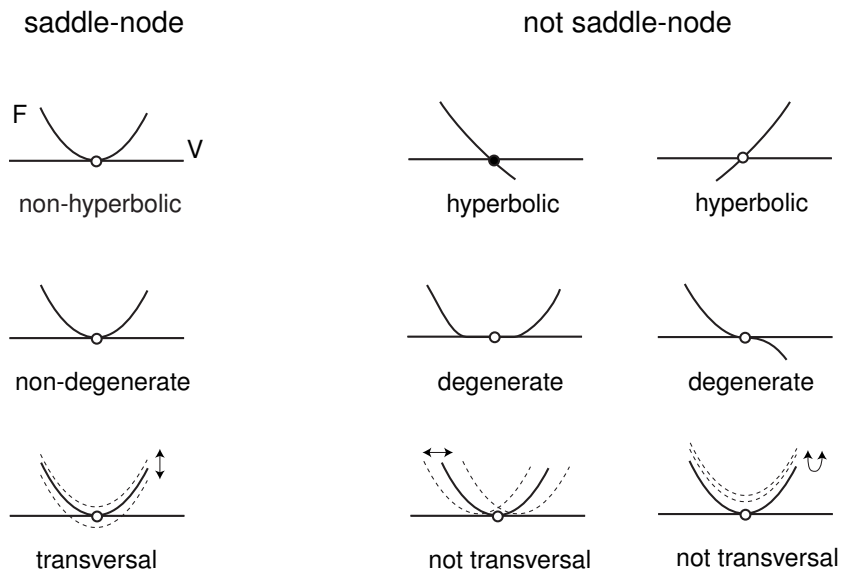

Figure 3.27: Geometrical illustration of the three conditions defining saddle-node bifurcations. Arrows denote the direction of displacement of the function $F(V, I)$ as the bifurcation parameter I changes.

bifurcation) if the following mathematical conditions, illustrated in Fig. 3.27, are satisfied:

- (Non-hyperbolicity) The eigenvalue λ at V_{sn} is zero; that is,

$$\lambda = F_V(V, I_{sn}) = 0 \qquad (\text{at } V = V_{sn}),$$

  where F_V means the derivative of F with respect to V, that is, $F_V = \partial F/\partial V$. Equilibria with zero or pure imaginary eigenvalues are called non-hyperbolic. Geometrically, this condition implies that the graph of F has horizontal slope at the equilibrium.

- (Non-degeneracy) The second order derivative with respect to V at V_{sn} is non-zero; that is,
$$F_{VV}(V, I_{sn}) \neq 0 \qquad (\text{at } V = V_{sn}).$$

  Geometrically, this means that the graph of F looks like the square parabola V^2 in Fig. 3.27.

- (Transversality) The function $F(V, I)$ is non-degenerate with respect to the bifurcation parameter I; that is,

$$F_I(V_{sn}, I) \neq 0 \qquad (\text{at } I = I_{sn}),$$

  where F_I means the derivative of F with respect to I. Geometrically, this means that while I changes past I_{sn}, the graph of F approaches, touches, and then intersects the V axis.

Saddle-node bifurcation results in appearance or disappearance of a pair of equilibria, as in Fig. 3.26. None of the six examples on the right-hand side of Fig. 3.27 can undergo a saddle-node bifurcation because at least one of the conditions above is violated.

The number of conditions involving strict equality ("=") is called the *co-dimension* of a bifurcation. The saddle-node bifurcation has *co-dimension-1* because there is only one condition involving "=", and the other two conditions involve inequalities ("≠"). Co-dimension-1 bifurcations can be reliably observed in systems with one parameter.

It is an easy exercise to check that the one-dimensional system

$$\dot{V} = I + V^2 \tag{3.9}$$

is at saddle-node bifurcation when $V = 0$ and $I = 0$ (please, check all three conditions). This system is called the *topological normal form* for saddle-node bifurcation. Phase portraits of this system are topologically equivalent to those depicted in Fig. 3.26 except that the bifurcation occurs at $I = 0$, and not at $I = 16$.
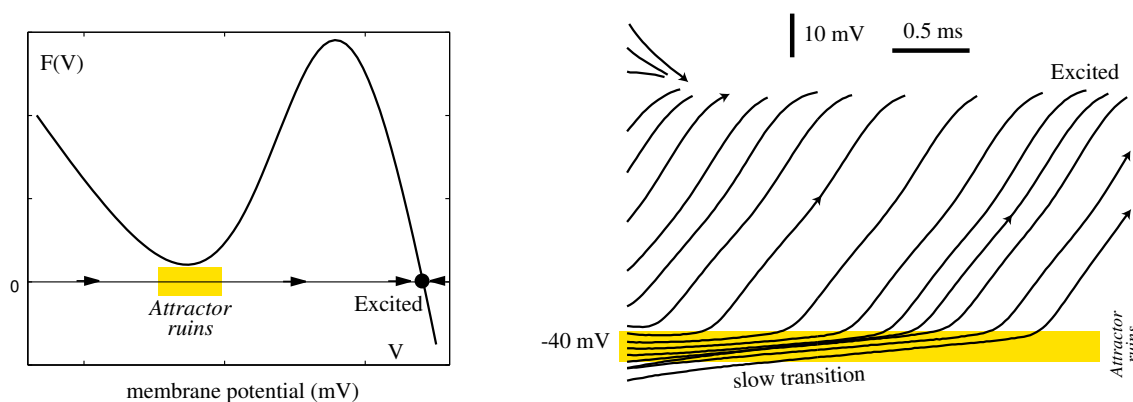
Figure 3.28: Slow transition through the ghost of the resting state attractor in cortical pyramidal neuron with $I = 30$ pA (the same neuron as in Fig. 3.15). Even though the resting state has already disappeared, the function $F(V)$, and hence the rate of change, $\dot{V}$, is still small when $V \approx -46$ mV.

3.3.5 Slow transition

All physical, chemical, and biological systems near saddle-node bifurcations possess certain universal features that do not depend on particulars of the systems. Consequently, all neural systems near such a bifurcation share common neuro-computational properties, which we will discuss in detail in Chapter 7. Here we glimpse one such property – slow transition through the ruins (or ghost) of the rest state attractor, which is relevant to the dynamics of many neocortical neurons.

In Fig. 3.28 we show the function $F(V)$ of the system (3.5) with $I = 30$ pA, which is greater than the bifurcation value 16 pA, and the corresponding behavior of the cortical neuron; compare with Fig. 3.15. The system has only one attractor – the excited state, and any solution starting from any initial condition should quickly approach this attractor. However, the solutions starting from the initial conditions around -50 mV do not seem to hurry. Instead, they slow down near -46 mV and spend quite some time in the voltage range corresponding to the resting state, as if the state were still present. The closer is I to the bifurcation value, the more time the membrane potential spends in the neighborhood of the resting state. Obviously, such a slow transition cannot be explained by a slow activation of the inward Na$^+$ current, since Na$^+$ activation in the cortical neuron is practically instantaneous.

The slow transition occurs because the neuron or the system (3.5) in Fig. 3.28 is near a saddle-node bifurcation. Even though I is greater than the bifurcation value, and the rest state attractor is already annihilated, the function $F(V)$ is barely above the V-axis at the "annihilation site". In other words, the rest state attractor has already been ruined, but its "ruins" (or its "ghost") can still be felt because

$$\dot{V} = F(V) \approx 0 \qquad \text{(at attractor ruins, } V \approx -46 \text{ mV),}$$

as one can see in Fig. 3.28. In Chapter 7 we will show how this property explains
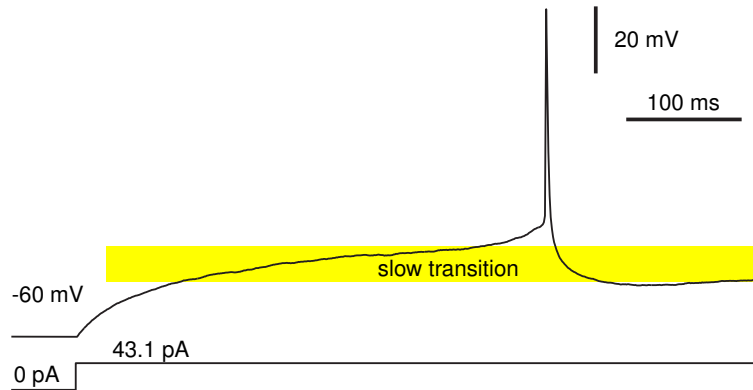
Figure 3.29: A 400-ms latency in layer 5 pyramidal neuron of rat visual cortex.
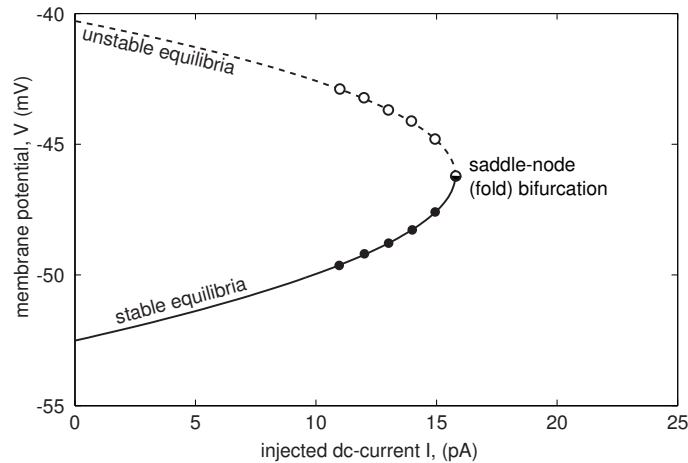

Figure 3.30: Bifurcation diagram of the system in Fig. 3.26.

the ability of many neocortical neurons, such as the one in Fig. 3.29, to generate repetitive action potentials with small frequency, and how it predicts that all such neurons considered as dynamical systems reside near saddle-node bifurcations.

3.3.6   Bifurcation diagram

The final step in the geometrical bifurcation analysis of one-dimensional systems is analysis of the bifurcation diagrams, which we do in Fig. 3.30 for the saddle-node bifurcation in Fig. 3.26. To make the bifurcation diagram, we determine the locations of the stable and unstable equilibria for each value of the parameter I and plot them as white or black circles in the (I, V) plane in Fig. 3.30. The equilibria form two branches that join at the fold point corresponding to the saddle-node bifurcation (hence the alternative name – *fold* bifurcation). The branch corresponding to the unstable equilibria is dashed to stress its instability. As the bifurcation parameter I varies from left to right through the bifurcation point, the stable and unstable equilibria coalesce
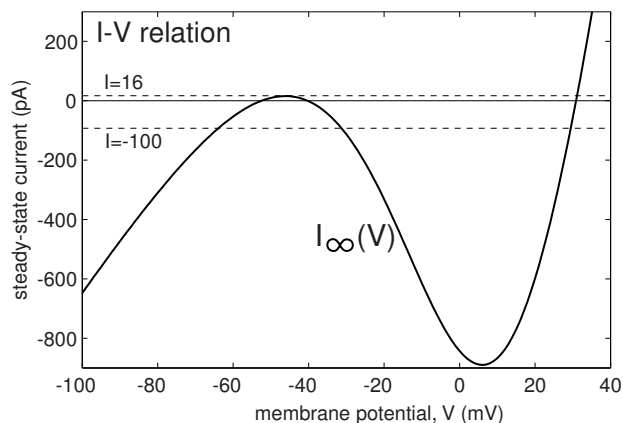
Figure 3.31: Equilibria are intersections of the steady-state I-V curve $I_\infty(V)$ and a horizontal line $I = \text{const.}$

and annihilate each other. As the parameter varies from right to left, two equilibria – one stable and one unstable – appear from a single point. Thus, depending on the direction of movement of the bifurcation parameter, the saddle-node bifurcation explains disappearance or appearance of a new stable state. In any case, the qualitative behavior of the systems changes exactly at the bifurcation point.

3.3.7 Bifurcations and I-V recordings

In general, determining saddle-node bifurcation diagrams of neurons may be a daunting mathematical task. However, it is a trivial exercise when the bifurcation parameter is the injected dc-current I. In this case, the bifurcation diagram, such as the one in Fig. 3.30, is just the steady-state I-V relation $I_\infty(V)$ plotted on the (I, V)-plane. Indeed, the equation

$$C\dot{V} = I - I_\infty(V) = 0$$

states that V is an equilibrium if and only if the net membrane current, $I - I_\infty(V)$, is zero. For example, equilibria of the $I_{\text{Na,p}}$-model are solutions of the equation

$$0 = I - \overbrace{(g_{\text{L}}(V - E_{\text{L}}) + g_{\text{Na}}m_\infty(V)(V - E_{\text{Na}}))}^{I_\infty(V)},$$

which follows directly from (3.5). In Fig. 3.31 we illustrate how to find the equilibria geometrically: We plot the steady-state I-V curve $I_\infty(V)$ and draw a horizontal line with altitude I. Any intersection satisfies the equation $I = I_\infty(V)$, and hence is an equilibrium (stable or unstable). Obviously, when I increases past 16, the saddle-node bifurcation occurs.

Notice that the equilibria are points on the curve $I_\infty(V)$, so flipping and rotating the curve by 90°, as we do in Fig. 3.32, left, results in a complete saddle-node bifurcation diagram. The diagram conveys in a very condensed manner all important information about the qualitative behavior of the $I_{\text{Na,p}}$-model. The three branches of the S-shaped curve, which is the 90°-rotated and flipped copy of the N-shaped I-V curve, correspond to the rest, threshold, and excited states of the model. Each slice $I = \text{const}$ represents
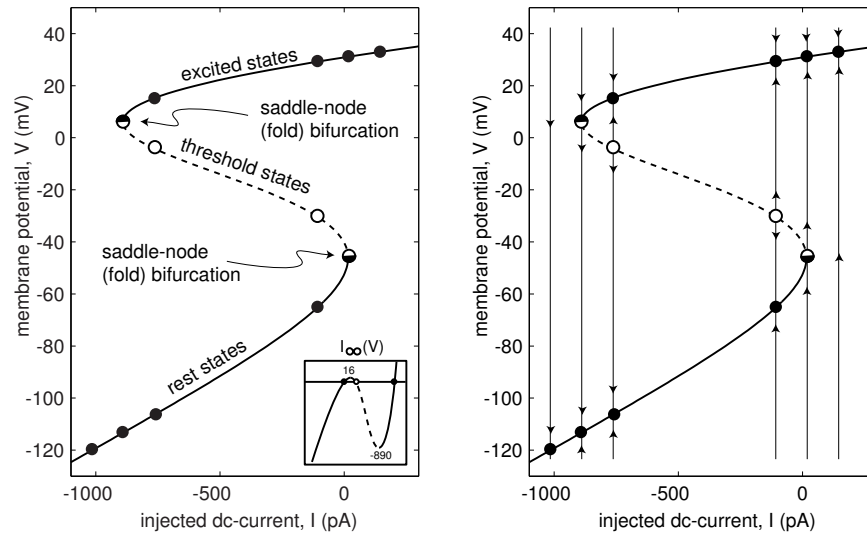
Figure 3.32: Bifurcation diagram of the $I_{\mathrm{Na,p}}$-model (3.5).

the phase portrait of the system, as we illustrate in Fig. 3.32, right. Each point where the branches fold (max or min of $I_{\infty}(V)$) corresponds to the saddle-node bifurcation. Since there are two such folds, at $I = 16$ pA and at $I = -890$ pA, there are two saddle-node bifurcations in the system. The first one studied in Fig. 3.25 corresponds to the disappearance of the rest state. The other one illustrated in Fig. 3.33 corresponds to the disappearance of the excited state. It occurs because I becomes so negative that the Na$^+$ inward current is no longer enough to balance the leak outward current and the negative injected dc-current to keep the membrane in the depolarized (excited) state.

Below the reader can find more examples of bifurcation analysis of the $I_{\mathrm{Na,p}}$- and I_{Kir}-models, which have non-monotonic I-V relations and can exhibit multi-stability of states. The I_{K}- and I_{h}-models have monotonic I-V relations and hence only one state. These models cannot have saddle-node bifurcations, as the reader is asked to prove in Ex. 14 and 15.

3.3.8   Quadratic integrate-and-fire neuron

Let us consider the topological normal form for the saddle-node bifurcation (3.9). From $0 = I + V^2$ we find that there are two equilibria, $V_{\mathrm{rest}} = -\sqrt{|I|}$ and $V_{\mathrm{thresh}} = +\sqrt{|I|}$ when $I < 0$. The equilibria approach and annihilate each other via saddle-node bifurcation when $I = 0$, so there are no equilibria when $I > 0$. In this case, $\dot{V} \geq I$ and $V(t)$ increases to infinity. Because of the quadratic term, the rate of increase also increases, resulting in a positive feedback loop corresponding to the regenerative activation of Na$^+$ current. In Ex. 16 we show that $V(t)$ escapes to infinity in a finite time, which corresponds to the up-stroke of the action potential. The same up-stroke is generated when $I < 0$, if the voltage variable is pushed beyond the threshold value V_{thresh}.
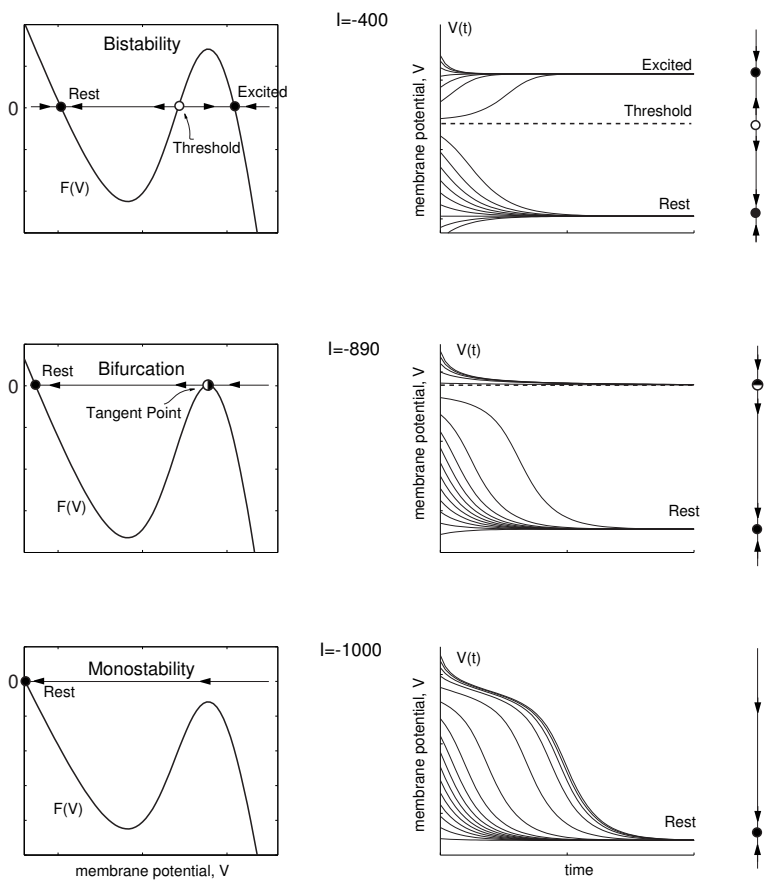
Figure 3.33: Bifurcation in the $I_{\text{Na,p}}$-model (3.5): The excited state and the threshold state coalesce and disappear when the parameter I is sufficiently small.
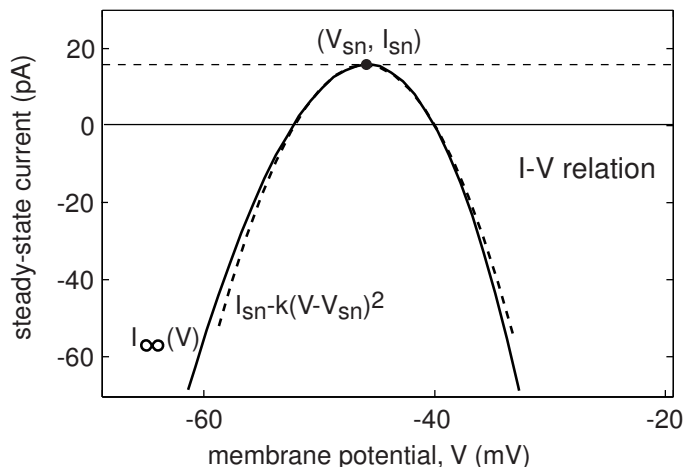
Figure 3.34: Magnification of the I-V curve in Fig. 3.31 at the left knee shows that it can be approximated by a square parabola.

Considering infinite values of the membrane potential may be convenient from a purely mathematical point of view, but this has no physical meaning and no way to simulate it on a digital computer. Instead, we fix a sufficiently large constant V_{peak} and say that (3.9) generated a spike when $V(t)$ reached V_{peak}. After the peak of the spike is reached, we reset $V(t)$ to a new value V_{reset}. The topological normal form for the saddle-node bifurcation with the after-spike resetting

$$\dot{V} = I + V^2 , \qquad \text{if } V \geq V_{\text{peak}}, \quad \text{then } V \leftarrow V_{\text{reset}} \qquad (3.10)$$

is called the *quadratic integrate-and-fire neuron.* It is the simplest model of a spiking neuron. The name stems from its resemblance to the *leaky* integrate-and-fire neuron $\dot{V} = I - V$ considered in Chap. 8. In contrast to the common folklore, the leaky neuron is not a *spiking model* because it does not have a spike-generation mechanism, i.e., a regenerative up-stroke of the membrane potential, whereas the quadratic neuron does. We discuss this and other issues in detail in Chap. 8.

In general, quadratic integrate-and-fire model could be derived directly from the equation $C\dot{V} = I - I_{\infty}(V)$ by approximating the steady-state I-V curve near the resting state by the square parabola $I_{\infty}(V) \approx I_{\text{sn}} - k(V - V_{\text{sn}})^2$, where $k > 0$ and the peak of the curve $(V_{\text{sn}}, I_{\text{sn}})$ could be easily found experimentally; see Fig. 3.34. Approximating the I-V curve by other functions, for example $I_{\infty}(V) = g_{\text{leak}}(V - V_{\text{rest}}) - ke^{pV}$, results in other forms of the model, e.g., the exponential integrate-and-fire model (Fourcaud-Trocme et al. 2003), which has certain advantages over the quadratic form. Unfortunately, the model is not solvable analytically, and it is expensive to simulate. The form $I_{\infty}(V) = g_{\text{leak}}(V - V_{\text{leak}}) - k(V - V_{\text{th}})_+^2$, where $x_+ = x$ when $x > 0$ and $x_+ = 0$ otherwise, combines the advantages of both models. The parameters V_{peak} and V_{reset} are derived from the shape of the spike. Normalization of variables and parameters results in the form (3.10) with $V_{\text{peak}} = 1$.

In Fig. 3.35 we simulated the quadratic integrate-and-fire neuron to illustrate a
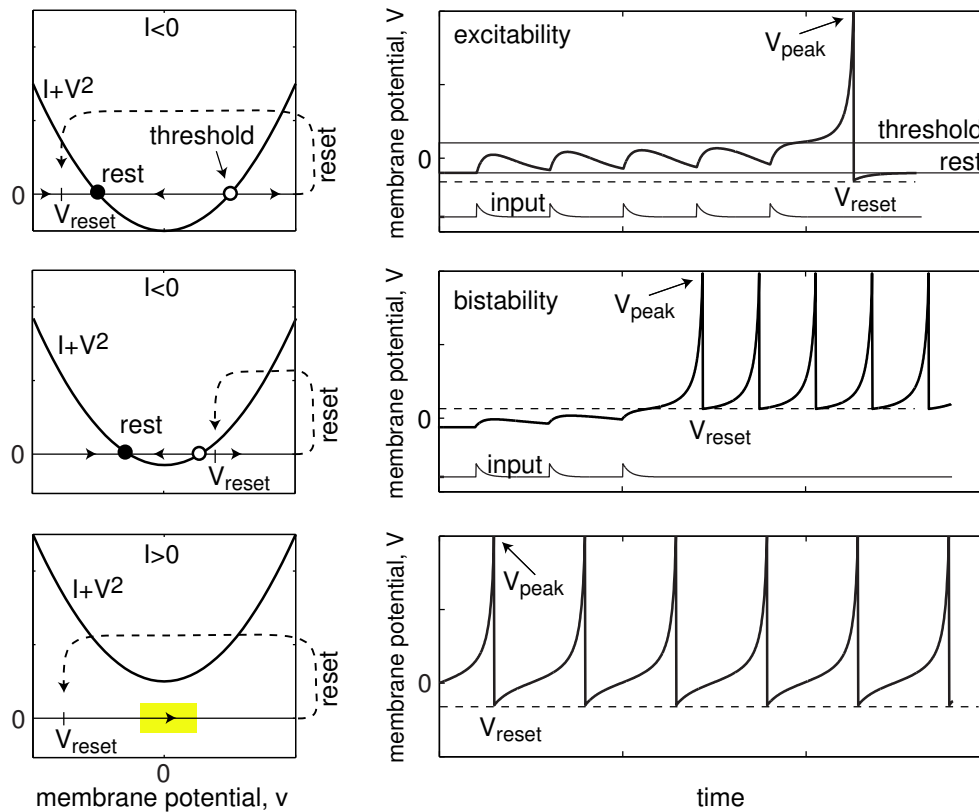
Figure 3.35: Quadratic integrate-and-fire neuron (3.10) with time-dependent input.

number of its features, which will be described in detail in subsequent chapters using conductance-based models. First, the neuron is an integrator; each input pulse in Fig. 3.35, top, pushes V closer to the threshold value; the higher the frequency of the input, the sooner V reaches the threshold and starts the up-stroke of a spike. The neuron is monostable when $V_{\text{reset}} \leq 0$ and could be bistable otherwise. Indeed, the first spike in Fig. 3.35, middle, is evoked by the input, but the subsequent spikes occur because the reset value is superthreshold.

The neuron could be Class 1 or Class 2 excitable depending on the sign of V_{reset}. Suppose the injected current I slowly ramps up from a negative to a positive value. The membrane potential follows the resting state $-\sqrt{|I|}$ in a quasi-static fashion until the bifurcation point $I = 0$ is reached. At this moment, the neuron starts to fire tonic spikes. In the monostable case $V_{\text{reset}} < 0$ in Fig. 3.35, bottom, the membrane potential is reset to the left of the ghost of the saddle-node point (see Sect. 3.3.5), thereby producing spiking with an arbitrary small frequency and hence Class 1 excitability. Because of the recurrence, such a bifurcation is called saddle-node on invariant circle. Many pyramidal neurons in mammalian neocortex exhibit such a bifurcation. In contrast, in the bistable case $V_{\text{reset}} > 0$, not shown in the figure, the membrane potential is reset to the right of the ghost, no slow transition is involved, and the tonic spiking starts with a non-zero frequency. As an exercise, explain why there is a noticeable latency (delay) to the first

spike right after the bifurcation. This type of behavior is typical in spiny projection neurons of neostriatum and basal ganglia, as we show in Chap. 8.

Review of Important Concepts

- One-dimensional dynamical system $\dot{V} = F(V)$ describes how the rate of change of V depends on V. Positive $F(V)$ means V increases, negative $F(V)$ means V decreases.

- In the context of neuronal dynamics, V is often the membrane potential, and $F(V)$ is the steady-state I-V curve taken with the minus sign.

- A zero of $F(V)$ corresponds to an equilibrium of the system. (Indeed, if $F(V) = 0$, then the state of the system, V, neither increases nor decreases.)

- An equilibrium is stable when $F(V)$ changes the sign from "+" to "-". A sufficient condition for stability is that the eigenvalue $\lambda = F'(V)$ at the equilibrium be negative.

- A phase portrait is a geometrical representation of the system's dynamics. It depicts all equilibria, their stability, representative trajectories, and attraction domains.

- A bifurcation is a qualitative change of the system's phase portrait.

- The saddle-node (fold) is a typical bifurcation in one-dimensional systems: As a parameter changes, a stable and an unstable equilibrium approach, coalesce, and then annihilate each other.

Bibliographical Notes

There is no standard textbook on dynamical systems theory. The classical book *Nonlinear Oscillations, Dynamical Systems, and Bifurcations of Vector Fields* by Guckenheimer and Holmes (1983) plays the same role in the dynamical systems community as the book *Ionic Channels and Excitable Membranes* by Hille (2001) in the neuroscience community. A common feature of these books is that they are not suitable as a first reading on the subject.

Most textbooks on differential equations, such as *Differential Equations and Dynamical Systems* by Perko (1996), develop the theory starting with the comprehensive analysis of linear systems, then applying it to local analysis of non-linear systems, and then discussing global behavior. By the time the reader gets to bifurcations, he has to go through a lot of daunting math, which is fun only for mathematicians. Here we

follow approach similar to *Nonlinear Dynamics and Chaos* by Strogatz (1994): Instead of going from linear to non-linear systems, we go from one-dimensional non-linear systems (this chapter) to two-dimensional non-linear systems (next chapter). Instead of providing the theory with a lot of mathematics, we use the geometrical approach to provoke the reader's intuition. (There is plenty of fun math in exercises and in the later chapters.)

Exercises

1. Consider a neuron having Na^+ current with fast activation kinetics. Assume that inactivation of this current, as well as (in)activations of the other currents in the neuron are much slower. Prove that the initial segment of action potential up-stroke of this neuron can be approximated by the $I_{Na,p}$-model (3.5). Use Fig. 3.15 to discuss the applicability of this approximation.

2. Draw phase portraits of the systems in Fig. 3.36. Clearly mark all equilibria, their stability, attraction domains, and direction of trajectories. Determine the signs of eigenvalues at each equilibrium.
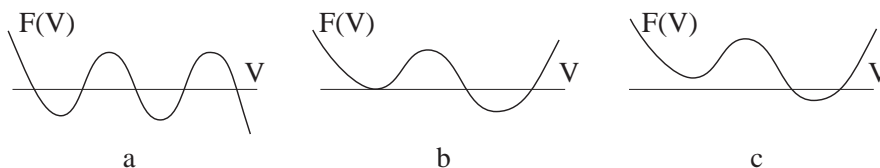

Figure 3.36: Draw phase portrait of the system $\dot{V} = F(V)$ with shown $F(V)$.

3. Draw phase portraits of the following systems

   (a) $\dot{x} = -1 + x^2$
   (b) $\dot{x} = x - x^3$

   Determine the eigenvalues at each equilibrium.

4. Determine stability of the equilibrium $x = 0$ and draw phase portraits of the following piece-wise continuous systems

$$
\text{(a)} \quad \dot{x} = \begin{cases} 2x, & \text{if } x < 0 \\ x, & \text{if } x \geq 0 \end{cases}
$$

$$
\text{(b)} \quad \dot{x} = \begin{cases} -1, & \text{if } x < 0 \\ 0, & \text{if } x = 0 \\ 1, & \text{if } x > 0 \end{cases}
$$

$$
\text{(c)} \quad \dot{x} = \begin{cases} -2/x, & \text{if } x \neq 0 \\ 0, & \text{if } x = 0 \end{cases}
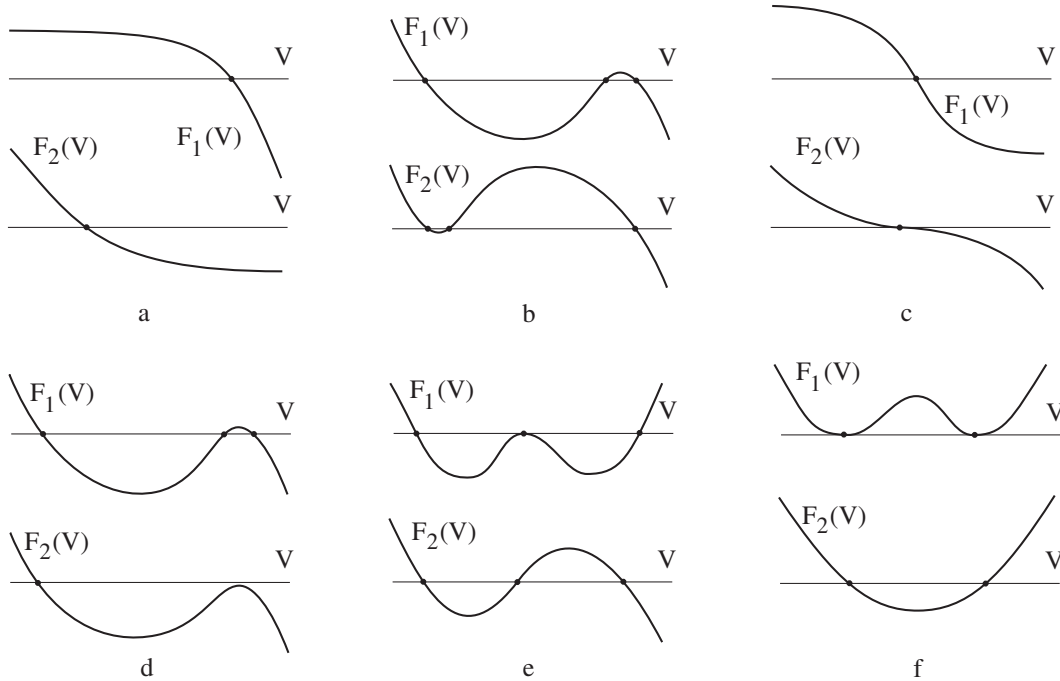$$

Figure 3.37: Which of the pairs correspond to topologically equivalent dynamical systems? (All intersections with the V axis are marked as dots.)

5. Draw phase portraits of the systems in Fig. 3.37. Which of the pairs in the figure correspond to topologically equivalent dynamical systems?

6. (Saddle-node bifurcation) Draw bifurcation diagram and representative phase portraits of the system $\dot{x} = a + x^2$, where a is a bifurcation parameter. Find the eigenvalues at each equilibrium.

7. (Saddle-node bifurcation) Use definition in Sect. 3.3.4 to find saddle-node bifurcation points in the following systems:

   (a) $\dot{x} = a + 2x + x^2$
   (b) $\dot{x} = a + x + x^2$
   (c) $\dot{x} = a - x + x^2$
   (d) $\dot{x} = a - x + x^3$ (Hint: verify the non-hyperbolicity condition first)
   (e) $\dot{x} = 1 + ax + x^2$
   (f) $\dot{x} = 1 + 2x + ax^2$

   where a is the bifurcation parameter.

8. (Pitchfork bifurcation) Draw bifurcation diagram and representative phase portraits of the system $\dot{x} = bx - x^3$, where b is a bifurcation parameter. Find the eigenvalues at each equilibrium.
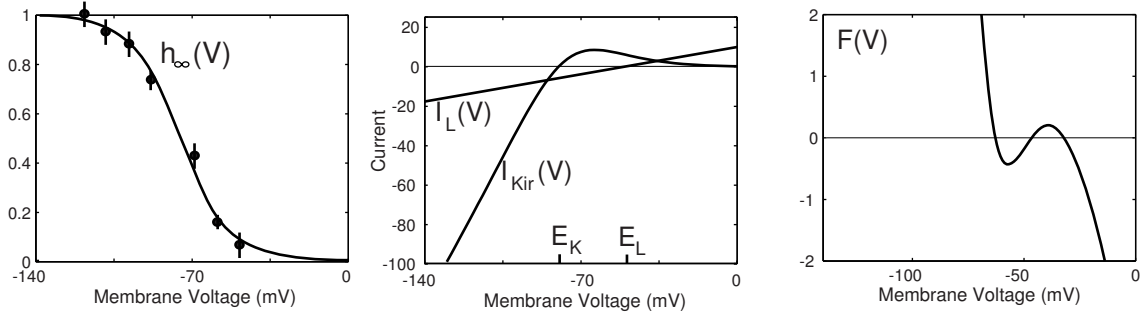
Figure 3.38: The I_{Kir}-model having injected current (I), leak current (I_{L}), and instantaneous K$^+$ inward rectifier current (I_{Kir}) and described by (3.11). Inactivation curve $h_\infty(V)$ is modified from Wessel et. al (1999). Parameters: $C = 1$, $I = 6$, $g_{\text{L}} = 0.2$, $E_{\text{L}} = -50$, $g_{\text{Kir}} = 2$, $E_{\text{K}} = -80$, $V_{1/2} = -76$, $k = -12$ (see Fig. 2.20).
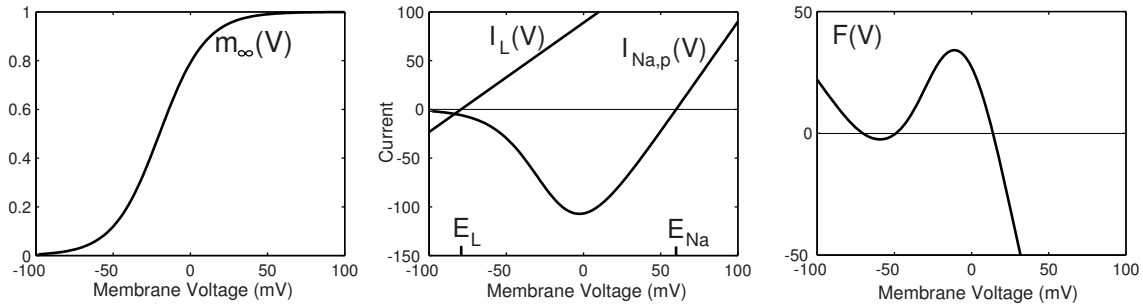

Figure 3.39: The $I_{\text{Na,p}}$-model having leak current (I_{L}) and persistent Na$^+$ current ($I_{\text{Na,p}}$) and described by (3.5) with the right-hand side function $F(V)$. Parameters: $C = 1$, $I = 0$, $g_{\text{L}} = 1$, $E_{\text{L}} = -80$, $g_{\text{Na}} = 2.25$, $E_{\text{Na}} = 60$, $V_{1/2} = -20$, $k = 15$ (see Fig. 2.20).

9. Draw bifurcation diagram of the I_{Kir}-model

$$C\dot{V} = I - g_{\text{L}}(V - E_{\text{L}}) - \overbrace{g_{\text{Kir}}h_\infty(V)(V - E_{\text{K}})}^{\text{instantaneous } I_{\text{Kir}}}, \qquad (3.11)$$

using parameters from Fig. 3.38 and treating I as a bifurcation parameter.

10. Derive an explicit formula that relates the position of the equilibrium in the Hodgkin-Huxley model to the magnitude of the injected dc-current I. Are there any saddle-node bifurcations?

11. Draw bifurcation diagram of the $I_{\text{Na,p}}$-model (3.5) using parameters from Fig. 3.39 and treating

   (a) g_{L} as a bifurcation parameter,
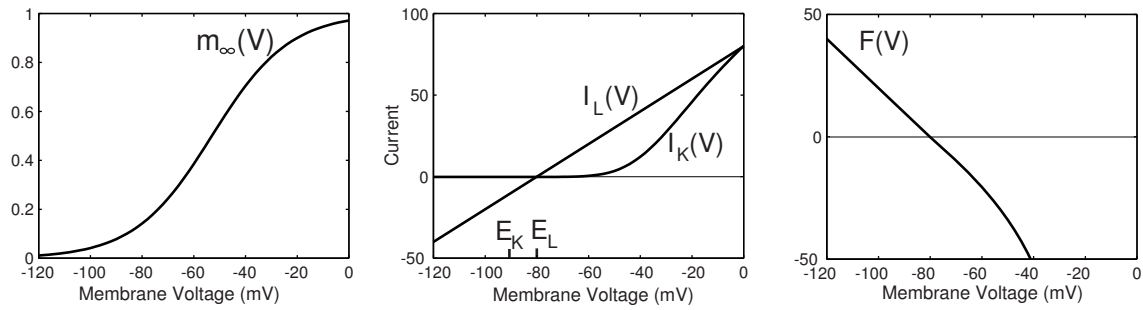   (b) E_{L} as a bifurcation parameter.

Figure 3.40: The I_K-model having leak current (I_L) and persistent K$^+$ current (I_K) and described by (3.12). Parameters: $C = 1$, $g_L = 1$, $E_L = -80$, $g_K = 1$, $E_K = -90$, $V_{1/2} = -53$, $k = 15$ (see Fig. 2.20).
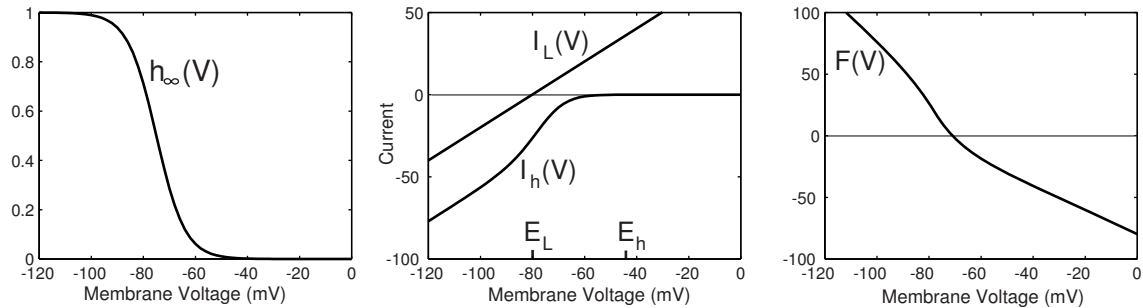

Figure 3.41: The I_h-model having leak current (I_L) and "hyperpolarization-activated" inward current I_h and described by (3.13). Parameters: $C = 1$, $g_L = 1$, $E_L = -80$, $g_h = 1$, $E_h = -43$, $V_{1/2} = -75$, $k = -5.5$ (Huguenard and McCormick 1992).

12. Draw bifurcation diagram of the I_{Kir}-model (3.11) using parameters from Fig. 3.38 and treating

    (a) g_L as a bifurcation parameter,

    (b) g_{Kir} as a bifurcation parameter.

13. Perform the bifurcation analysis of the $I_{Na,p}$-model with $I = 0$ and g_{Na} as a bifurcation parameter. In particular, use computer simulations to reproduce analogues of figures 3.25, 3.26, and 3.30–3.33.

14. Show that the I_K-model in Fig. 3.40

$$C\dot{V} = -g_L(V - E_L) - \overbrace{g_K m_\infty^4(V)(V - E_K)}^{\text{instantaneous } I_K} . \qquad (3.12)$$

cannot exhibit saddle-node bifurcation for $V > E_K$. (Hint: show that $F'(V) \neq 0$ for all $V > E_K$.)

15. Show that the I_h-model in Fig. 3.41

$$C\dot{V} = -g_\mathrm{L}(V - E_\mathrm{L}) - \overbrace{g_\mathrm{h}h_\infty(V)}^{\text{instantaneous } I_\mathrm{h}}(V - E_\mathrm{h}) \qquad (3.13)$$

cannot exhibit saddle-node bifurcation for any $V < E_\mathrm{h}$.

16. Prove that the upstroke of the spike in the quadratic integrate-and-fire neuron (3.9) has the asymptote $1/(c - t)$ for some $c > 0$.

17. (Cusp bifurcation) Draw bifurcation diagram and representative phase portraits of the system $\dot{x} = a + bx - x^3$, where a and b are bifurcation parameters. Plot the bifurcation diagram in the (a, b, x)-space and on the (a, b)-plane.

18. (Gradient systems) An n-dimensional dynamical system $\dot{x} = f(x)$, $x = (x_1, \ldots, x_n) \in \mathbb{R}^n$ is said to be *gradient* when there is a potential (energy) function $E(x)$ such that

$$\dot{x} = -\operatorname{grad} E(x) ,$$

where

$$\operatorname{grad} E(x) = (E_{x_1}, \ldots, E_{x_n})$$

is the gradient of $E(x)$. Show that all one-dimensional systems are gradient (Hint: see Fig. 3.11). Find potential (energy) functions for the following one-dimensional systems

a. $\dot{V} = 0$	b. $\dot{V} = 1$	c. $\dot{V} = -V$
d. $\dot{V} = -1 + V^2$	e. $\dot{V} = V - V^3$	f. $\dot{V} = -\sin V$

19. Consider a dynamical system $\dot{x} = f(x)$, $x(0) = x_0$.

(a) (Stability) An equilibrium y is *stable* if any solution $x(t)$ with x_0 sufficiently close to y remains near y for all time. That is, for all $\varepsilon > 0$ there exists $\delta > 0$ such that if $|x_0 - y| < \delta$ then $|x(t) - y| < \varepsilon$ for all $t \geq 0$.

(b) (Asymptotic stability) A stable equilibrium y is *asymptotically stable* if all solutions starting sufficiently close to y approach it as $t \to \infty$. That is, if $\delta > 0$ from the definition above could be chosen so that $\lim_{t\to\infty} x(t) = y$.

(c) (Exponential stability) A stable equilibrium y is said to be *exponentially stable* when there is a constant $a > 0$ such that $|x(t) - y| < \exp(-at)$ for all x_0 near y and all $t \geq 0$.

Prove that (c) implies (b), and (b) implies (a). Show that (a) does not imply (b) and (b) does not imply (c); That is, present a system having stable but not asymptotically stable equilibrium, and a system having asymptotically but not exponentially stable equilibrium.